ELSEVIER

Journal of Structural Geology 27 (2005) 1252–1281

JOURNAL OF STRUCTURAL GEOLOGY

www.elsevier.com/locate/jsg

The northern Inner Piedmont, southern Appalachians, USA: kinematics of transpression and SW-directed mid-crustal flow

Arthur J. Merschat[a,*], Robert D. Hatcher Jr[a], Timothy L. Davis[b]

[a]*Department of Earth and Planetary Sciences, University of Tennessee-Knoxville, 306 Earth and Planetary Sciences Building, Knoxville, TN 37996-1410, USA*
[b]*Occidental Oil and Gas Co., 5 Greenway Plaza, Suite 10, Houston, TX 77227-7757, USA*

Received 16 April 2003; accepted 17 June 2004
Available online 23 November 2004

Abstract

Analysis of new and existing field, structural, petrologic, and geochronologic data in the northern Inner Piedmont (IP), southern Appalachians, provide insight into the processes and kinematics of Neoacadian (Late Devonian–Mississippian) crustal flow. The IP is characterized by 360–345 Ma middle to upper amphibolite facies metamorphism, gentle dip of the dominant S_2 foliation, and curved L_2 mineral lineation pattern. Recognized map-scale sheath folds are cored by Henderson Gneiss or outlined by Devonian granitoids, and record SW-directed axial elongations of 120–486%. Net Neoacadian fault displacement exceeds 400 km, with over 200 km associated with SW-directed, orogen-parallel flow. Map-scale sheath folds and mineral lineation patterns suggest that NW- and W-directed flow rooted to the east was deflected SW by an oblique buttress in the footwall beneath the Neoacadian Brevard fault zone. Kinematic vorticity estimates remain in the realm of sub-simple shear across the IP, and approaches simple shear in the Neoacadian Brevard fault zone. Curved IP flow paths provide a model for middle to lower crustal deformation and flow in ancient to active orogens like the Himalayas, including the possibility that the IP is an exhumed orogenic channel.

Keywords: Appalachians; Inner Piedmont; Kinematic vorticity; Mid-Paleozoic crustal flow

1. Introduction

Continental lithosphere deforms in three dimensions, yet we mostly create two-dimensional kinematic and mechanical models of crustal deformation processes. Cross-sections through strongly curved segments of orogens, like the arc of the western Alps (Laubscher, 1991) and the Tennessee salient of the southern Appalachian foreland (Macedo and Marshak, 1999), may be restorable if taken singly, but are nearly impossible to properly restore if considered in 3-D throughout the entire arc. Cross-section analysis is of even more limited value in the more heterogeneously deformed internal parts of orogens, and should be undertaken with caution. Understanding these crustal processes requires devising kinematic models for macroscopic ductile flow in the internal portions of orogens in 3-D (Turner and Weiss, 1963; Laubscher, 1991; Azcárraga et al., 2002).

The southern Appalachians are a Paleozoic mountain chain composed of a deformed rifted margin and platform to which an array of both suspect and exotic terranes were accreted during: the Taconic (Middle–Late Ordovician), Acadian (Devonian)–Neoacadian (Devonian–Mississippian), and Alleghanian (Pennsylvanian–Permian) orogenies. The Inner Piedmont (IP) consists of a middle to upper amphibolite facies assemblage of para- and orthogneisses that extends from northern North Carolina to the Coastal Plain in Alabama wherein the dominant foliation has a characteristic gentle dip (Figs. 1 and 2). Bream et al. (2001) and Bream and Hatcher (2002) have refined the IP terrane assemblage, based on new structural and geochronologic data, separating the Cat Square terrane of Siluro–Devonian rocks in the eastern IP from the former eastern part of the Tugaloo terrane. This paper addresses the 3-D structural evolution of the high temperature and pressure Appalachian Neoacadian metamorphic core—the composite IP.

* Corresponding author. Fax: +1-865-974-9326.
E-mail address: amerscha@utk.edu (A.J. Merschat).

0191-8141/$ - see front matter © 2004 Elsevier Ltd. All rights reserved.
doi:10.1016/j.jsg.2004.08.005

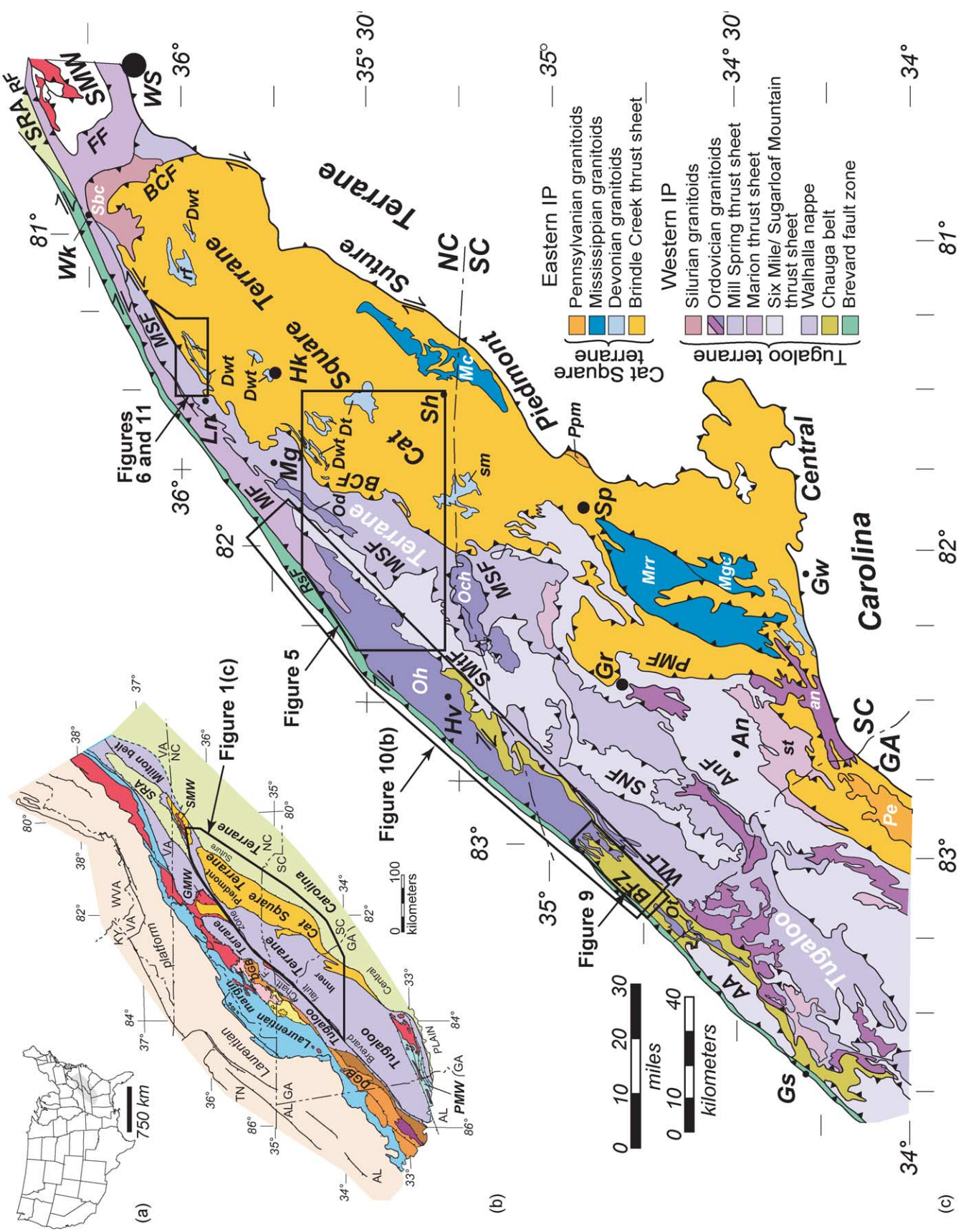
(a)
750 km
(b)
(c)
Figure 1(c)
Figure 5
Figure 10(b)
Figure 9
Figures 6 and 11
Eastern IP
Pennsylvanian granitoids
Mississippian granitoids
Devonian granitoids
Brindle Creek thrust sheet
Cat Square terrane
Western IP
Silurian granitoids
Ordovician granitoids
Mill Spring thrust sheet
Marion thrust sheet
Six Mile/ Sugarloaf Mountain thrust sheet
Walhalla nappe
Chauga belt
Brevard fault zone
Tugaloo terrane
Carolina
Central
Piedmont
Suture
Terrane
Square
Cat
Tugaloo
Laurentian
platform
kilometers
miles
0 10 20 30
0 10 40
0 100 kilometers

Studies of the northern IP (from North Carolina to northern Georgia) during the past 15 years (Davis, 1993a,b; Yanagihara, 1994; Bream, 1999; Giorgis, 1999; Hill, 1999; Williams, 2000; Bier, 2001; Garihan, 2001; Hatcher, 2001; Kalbas, 2003) have contributed to resolving the spatial and temporal deformation plan of the IP. While Griffin (1967, 1969, 1971, 1974a) first recognized large recumbent fold thrusts in the IP, he concluded that the thrusts were consistently northwest vergent, and involved plane strain deformation. Goldsmith (1981) first pointed out the arcuate pattern of mineral lineations and early fold hinges (Fig. 2d) in the northern IP, which has become a cornerstone of our model. Our goals are to bring together both existing and new map- and mesoscale structural data, develop a compatible 3-D kinematic model for the IP, and consider the implications of this model for the 3-D evolution of the internal parts of mountain chains.

2. Tectonic setting and attributes of the northern IP

The IP is one of the largest sillimanite grade terranes in the world, extending from the Sauratown Mountains window near Winston-Salem, North Carolina to central Alabama where it terminates beneath the Coastal Plain (Bentley and Neathery, 1970; Rodgers, 1970; Brown et al., 1985; Hatcher, 1987, 1989, 1993; Osborne et al., 1988) (Fig. 1a). It is separated from the eastern Blue Ridge (western Tugaloo terrane) to the northwest by the Brevard fault zone (BFZ) and from the exotic Carolina terrane (Secor et al., 1983) to the southeast by the central Piedmont suture (Hatcher and Zietz, 1980; Williams and Hatcher, 1983) (Fig. 1). In general, the rocks consist of biotite gneiss/metagraywacke, aluminous schist, pelitic schist, amphibolite, quartzite, ultramafic rocks, and granitoids (King, 1955). Metamorphic grade remains at or above first sillimanite across the broad core of the IP, decreasing to kyanite and locally garnet grade on the eastern and western flanks (Butler, 1991).

The IP has long been characterized by shallow-dipping foliation (King, 1955; Rodgers, 1970) (Fig. 2) and more recently, a stack of gently dipping crystalline thrust sheets has been recognized (Griffin, 1971; Goldsmith et al., 1988; Higgins et al., 1988; Horton and McConnell, 1991). Griffin (1971) suggested that the IP is the autochthonous core of a high-grade nappe complex, but other interpretations favor allochthonous crystalline thrust sheets (e.g. Hatcher, 1972, 1974, 1978; Goldsmith et al., 1988; Higgins et al., 1988; Hatcher and Hooper, 1992; Nelson et al., 1998). Hatcher and Hooper (1992) concluded the IP thrusts are Type-F thrusts: plastic, lobate, fold-derived thrusts with penetrative mesofabrics that evolved entirely beneath the ductile–brittle transition, similar to those in the Parry Sound region of the southern Grenville province in Ontario (Hanmer, 1988), the Cabo Ortegal complex in northwestern Spain (Azcárraga et al., 2002), the Moine nappes in the northern Scottish Caledonides (Alsop and Holdsworth, 1999, 2002), and the Pennine Alpine nappes (Trümpy, 1960, 1980; Merle et al., 1989). Seven major faults occur in the northern IP (Fig. 1c), and additional thrust sheets have been recognized in the IP farther south in Georgia (Higgins et al., 1988).

3. Lithologies and terrane boundaries

The Brindle Creek fault extends from northwest of Winston-Salem, North Carolina to south of Athens, Georgia (Fig. 1c). It separates the IP into two contrasting lithologic assemblages: the western and eastern IP (Bream and Hatcher, 2002). Dominance of biotite gneiss/metagraywacke in the western IP versus aluminous schist and biotite gneiss in the eastern IP can be easily recognized on most geologic maps (e.g. Bryant and Reed, 1970; Brown et al., 1985; Goldsmith et al., 1988). Magmatism in the IP is also partitioned across the Brindle Creek fault: Ordovician–Silurian magmatism dominates to the west and Devonian–Mississippian magmatism dominates to the east (Mapes, 2002; Mapes et al., 2002). Based on the occurrence of 400, 500, and 600 Ma detrital zircons (in addition to 1.1–1.2 Ga detrital zircons) in biotite gneiss, Bream et al. (2001, 2004) concluded that the Brindle Creek fault is a terrane boundary separating Neoproterozic–early Paleozoic Laurentian affinity rocks of the western IP–Tugaloo terrane from suspect middle Paleozoic rocks of the eastern IP–Cat Square terrane

Fig. 1. (a) Index map of the U.S. (b) Tectonic map of the southern Appalachians showing the location of the Inner Piedmont and major tectonostratigraphic terranes. DGB—Dahlonega gold belt; GMW—Grandfather Mountain window; PMW—Pine Mountain window; SMW—Sauratown Mountains window; SRA—Smith River allochthon; Chatt. F.—Chattahoochee fault; Dark purple—Elkahatchee pluton (Middle Ordovician); Yellow, pink, light orange, and brown—internal Blue Ridge terranes; Red—Grenville and pre-Grenville basement. (c) Tectonic map of the Inner Piedmont in the Carolinas and northern Georgia, compiled and modified from Rankin et al. (1972), Espenshade et al. (1975), Goldsmith et al. (1988), Hopson and Hatcher (1988), Hatcher and Hooper (1992), Nelson et al. (1998), and fig. 1 in Hatcher (2002, and sources cited therein). Faults and thrust sheets: AA—Alto allochthon; AnF—Anderson; BCF—Brindle Creek; BFZ—Brevard; FF—Forbush; MF—Marion; MSF—Mill Spring; PMF—Paris Mountain; RF—Ridgeway; RsF—Rosman fault; SMtF—Sugarloaf Mountain fault; SMW—Sauratown Mountains window; SNF—Six Mile-Seneca; SRA—Smith River allochthon; WLF—Walhalla. Named Ordovician (purple) and Ordovician(?) (lighter purple) granitoids: Och—Caesars Head; Od—Dysartsville; Oh—Henderson; Ot—Toccoa; an—Antreville; st—Starr. Others in the western Inner Piedmont (probably Ordovician) are colored lighter shades of purple. Silurian granitoid: Sbc—Brooks Crossroads. Devonian and Devonian(?) plutons (light blue): rf—Rocky Face; Dt—Toluca; Dwt—Walker Top; sm—Sandy Mush; Darker blue—Mississippian plutons: Mc—Cherryville; Mgc—Gray Court; Mrr—Reedy River. Pennsylvanian plutons: Pe—Elberton; Ppm—Pacolet Mills (in Carolina terrane). Towns: An—Anderson; Gr—Greenville; Gs—Gainesville; Gw—Greenwood; Hk—Hickory; Hv—Hendersonville; Ln—Lenoir; Mg—Morganton; Sh—Shelby; Sp—Spartanburg; Wk—Wilkesboro; WS—Winston-Salem.

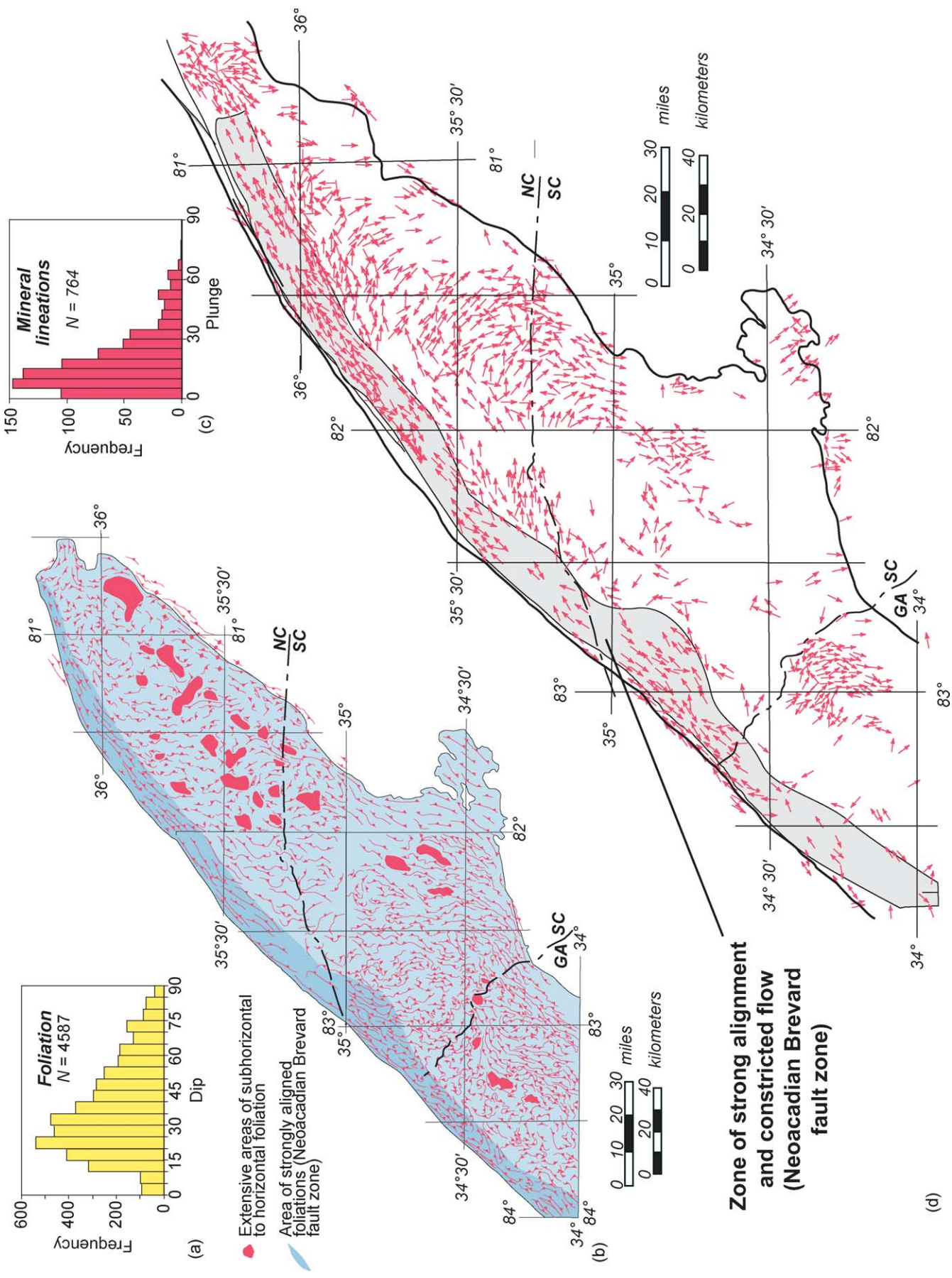
Foliation
N = 4587
Frequency
Dip
(a)
Extensive areas of subhorizontal to horizontal foliation
Area of strongly aligned foliations (Neoacadian Brevard fault zone)
NC
SC
GA
miles
kilometers
(b)
Mineral lineations
N = 764
Plunge
(c)
Zone of strong alignment and constricted flow (Neoacadian Brevard fault zone)
(d)

(Bream et al., 2001, 2004; Bream and Hatcher, 2002; Hatcher, 2002).

3.1. Western IP

Western IP rocks are part of the Tugaloo terrane, the western boundary of which is the Chattahoochee fault in the eastern Blue Ridge (Fig. 1b). The BFZ is located within this terrane and, because it was a suitably oriented crustal weak zone during Neoacadian deformation in the eastern Blue Ridge and IP, it had a long history of reactivation (Hatcher, 2001). The crustal affinity of the IP has long been debated, with some concluding that the BFZ is a suture, making the IP a suspect (Williams and Hatcher, 1983) or an exotic terrane (e.g. Rankin, 1975; Horton and McConnell, 1991; Hibbard, 2000). Detrital zircon data indicate Laurentian affinity of eastern and western Blue Ridge rocks indicating that the BFZ likely is not a suture (Bream et al., 2000, 2001; Bream, 2003). Identical stratigraphic sequences (Tallulah Falls Formation rocks) on both sides of the BFZ also preclude it being a suture (Hopson and Hatcher, 1988; Hatcher, 2001, 2002).

Western IP thrust sheets contain the Laurentian affinity, Neoproterozoic to Cambrian(?) Tallulah Falls and Chauga River Formations unconformably overlain by Middle Ordovician Poor Mountain Formation, traceable from near Gainesville, Georgia to northeast of Lenoir, North Carolina (Bream, 2002; Hatcher, 2002; Bream et al., 2004). The Tallulah Falls Formation consists of lower metagraywacke–amphibolite and upper metagraywacke units separated by a mappable aluminous schist unit (Hatcher, 1978, 1993). The Tallulah Falls Formation is overlain by graphitic phyllite and quartzite, muscovite–chlorite phyllite, impure marble and more chlorite–muscovite phyllite unique to the BFZ and phyllonitic metasiltstone southeast of the BFZ: the Chauga River Formation (Hatcher, 1969, 2002). These units yield only 1.1 Ga and older detrital zircons (Bream, 2002, 2003; Bream et al., 2004). Laminated to massive amphibolite (MORB to island-arc basalt composition) is overlain by quartzite–felsic tuff and marble of the Middle Ordovician Poor Mountain Formation, the youngest known unit in the western IP (Hatcher, 1969, 2002). New 460–440 Ma ion microprobe zircon ages on the amphibolite and felsic tuff (Bream, 2003), the absence of older zircons, and northeastward decreased thickness of Chauga River metasiltstone, suggest the Poor Mountain rests unconformably atop the Tallulah Falls and Chauga River Formations (Hatcher, 2002).

Tallulah Falls Formation rocks were intruded by the ~490 Ma (Carrigan et al., 2001) Henderson Gneiss (biotite-K-feldspar quartz monzonite augen gneiss) (Fig. 3a), and plagioclase-dominant 470–460 Ma granitoids, including the Dysartsville Tonalite, Sugarloaf Mountain gneiss, and Toccoa granitoid (Bream, 2002, 2003; Bream et al., 2004). These plutons occur intermittently from NE Georgia to north of Lenoir, North Carolina (Reed and Bryant, 1964; Bryant and Reed, 1970; Harper and Fullagar, 1981; Hatcher, 1993; Bream, 2003).

3.2. Eastern IP

Eastern IP–Cat Square terrane rocks consist of aluminous schist and metagraywacke intruded by Devonian to Carboniferous granitoids. The eastern IP paragneiss sequence contains detrital zircons as young as ~430 Ma, and the entire detrital zircon suite reveals a mixed Laurentian and Peri–Gondwanan provenance for this assemblage (Bream, 2002, 2003; Bream et al., 2004).

The Devonian and Carboniferous Toluca (378 Ma; Mapes, 2002), Walker Top (366 Ma; Mapes, 2002), and Cherryville Granites (375 Ma; Mapes, 2002) intruded the Cat Square terrane. The Toluca and Cherryville Granites are massive, equigranular, medium- to coarse-grained, foliated, and have concordant to subconcordant contacts. Chemically, all are intraplate, possibly anatectic granites (Giorgis et al., 2002; Mapes, 2002). The 366±4 Ma Walker Top Granite is porphyritic with microcline megacrysts 1–8 cm long (Giorgis et al., 2002; Mapes et al., 2002) (Fig. 3c and d).

4. Metamorphism

Metamorphic grade increases from garnet (in South Carolina) and staurolite–kyanite (in North Carolina) near the BFZ to sillimanite and higher grade across the broad core of the IP (Reed and Bryant, 1964; Bryant and Reed,

Fig. 2. Pattern of dominant (S_2) foliation and lineation in the northern Inner Piedmont. (a) Histogram of 4587 dip measurements of dominant foliation in the northern Inner Piedmont. (b) Form-line map of S_2 foliation in the northern Inner Piedmont. Form lines are parallel to strike; teeth on trend lines indicate dip direction. Density of form lines indicates density of data coverage used in map compilation. New data collected after this map was compiled reinforce the broad patterns depicted on this map. Based on 4587 measurements from Hadley and Nelson (1971), Rankin et al. (1972), Espenshade et al. (1975), Heyn (1984), Goldsmith et al. (1988), Nelson et al. (1998), and Hatcher (unpublished data). (c) Histogram of 764 mostly mineral lineations in the northern IP. Note the dominance of gentle plunges. (d) Distribution of measured lineations (filtered to create spacing). Arrowhead indicates direction of plunge; arrowhead on both ends of line indicates horizontal lineation. Line on each measurement indicates trend. Additional measurements added to this data set since the original compilation was made (see Figs. 7 and 12) reinforce the curved pattern illustrated by the data. Sources of lineation data are Grant (1958), Hadley and Nelson (1971), Lemmon and Dunn (1973a,b), Griffin (1974a), Whisonant (1979), Conley and Drummond (1981), Goldsmith (1981), Hatcher and Acker (1984), Heyn (1984), Hopson (1984), Willis (1984), Dennis (1989), McConnell (1990), Liu (1991), Davis (1993a), Maybin (1995, 1997), Niewendorp and Maybin (1994a,b), Yanagihara (1994), Niewendorp (1995a,b, 1996, 1997), West (1996, 1997, unpublished data), Curl (1998), Nelson et al. (1998), J.M. Garihan (unpublished data), R.D. Hatcher, Jr (unpublished data), and W.M. Schwerdtner (unpublished data).

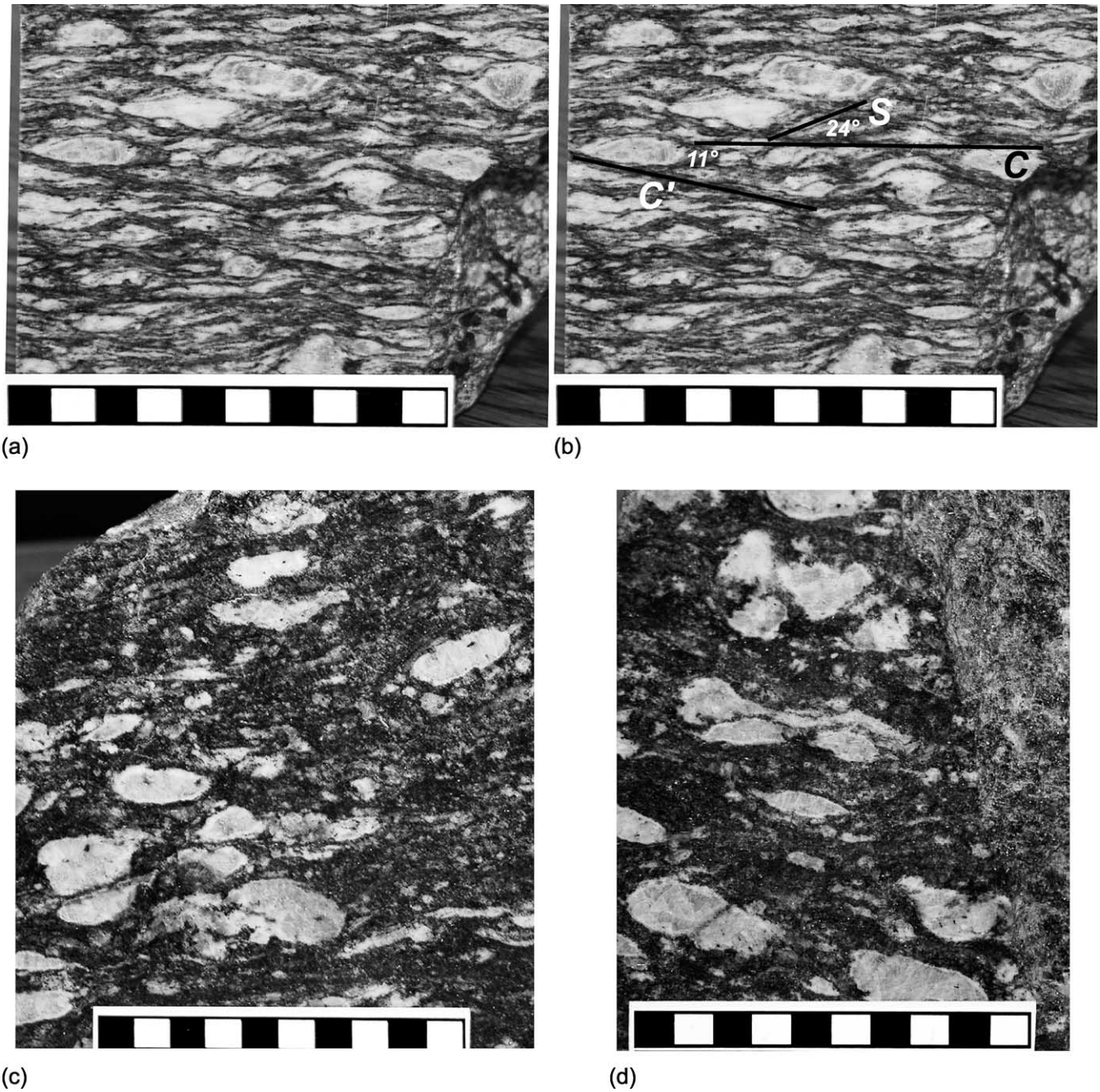

Fig. 3. Henderson Gneiss and Walker Top Granite. (a) and (b) Sawed surface of typical Henderson Gneiss from the Hendersonville, NC quarry containing abundant K-feldspar augen with dextral shear sense. The dominant foliation is a C foliation; a C′ foliation is inclined ~11° to C, while a relict S foliation can be seen at ~24° to C. (c) Sawed specimen of Walker Top Granite from south of Morganton, NC, containing partially deformed K-feldspar megacrysts, most of which have white myrmekite reaction rims, in a foliated biotite–quartz–plagioclase groundmass. (d) Different sawed surface on the same specimen as in (c). Scale bars have 1 cm subdivisions.

1970; Butler, 1991; Bier et al., 2002), locally decreasing to staurolite or garnet grade along the southeast flank (Goldsmith et al., 1988; Butler, 1991) (Fig. 4a). IP rocks are pervasively migmatitic, except along the flanks. P–T estimates range from 500–800 °C and 3–7 kbar (Davis, 1993a; Mirante and Patino-Douce, 2000; Bier et al., 2002; Merschat, 2003) (Fig. 4b). Single continuous garnet zoning profiles and an increase in temperature from garnet cores to rims from both the western and eastern IP indicate that the IP underwent a single prograde metamorphic event (Davis, 1993a; Bier et al., 2002; Merschat and Kalbas, 2002). Retrograde greenschist facies assemblages result from Alleghanian reactivation of the BFZ (Reed and Bryant, 1964; Bryant and Reed, 1970; Hatcher, 2001).

Hopson and Hatcher (1988) documented fault-related inversion of metamorphic isograds beneath the Alto

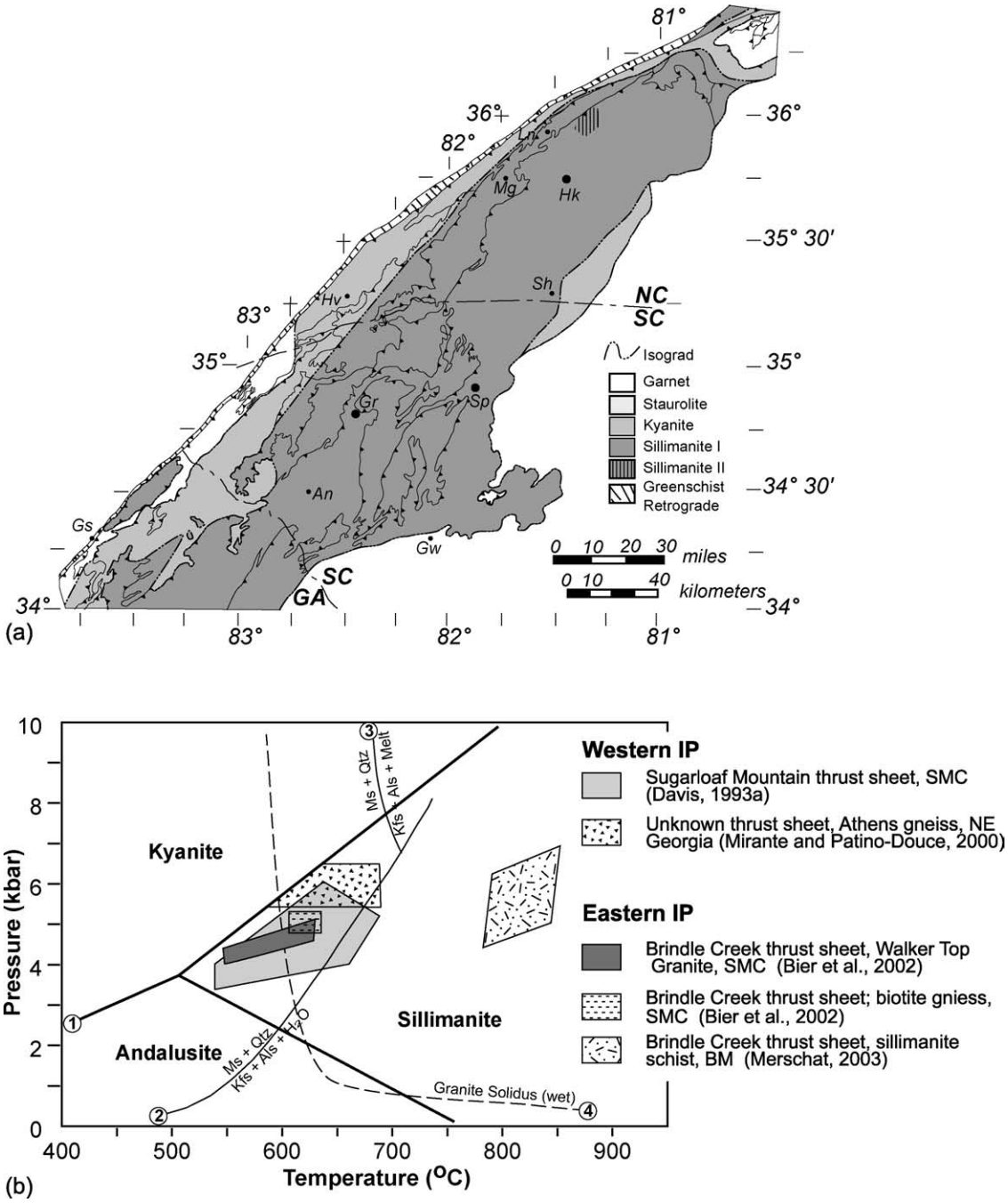

Fig. 4. (a) Metamorphic isograd map for the northern IP. Modified from Butler (1991) and Hatcher and Goldberg (1991). (b) P–T estimates for the northern IP compiled from Davis (1993a), Mirante and Patino-Douce (2000), Bier et al. (2002), and Merschat (2003). Numbered univariant lines from: (1) Holdaway (1971); (2) Chatterjee and Johannes (1974); (3) Thompson (1982); (4) Luth et al. (1964). Qtz—quartz; Ms—muscovite; Kfs—potassium feldspar; Als—aluminum silicate.

allochthon in northeast Georgia and northwestern South Carolina. Rocks of the Brindle Creek fault footwall are intensely migmatitic up to 7 km west of the trace of the fault (Giorgis, 1999; Merschat and Kalbas, 2002). Hatcher (2002) and Merschat and Kalbas (2002) speculated the sheet was emplaced hot and the additional heat and crustal thickening summed to produce the intense footwall migmatization. Griffin (1969) observed a similar phenomenon locally beneath the Six Mile thrust sheet.

Using conventional (TIMS) U–Pb dating methods, Dennis and Wright (1997a,b) reported monazite ages of ~360 and ~325 Ma from a sample traverse across the South Carolina IP. Mirante and Patino-Douce (2000) reported an electron microprobe U–Pb monazite age of ~330 Ma for IP metamorphism near Athens, Georgia. Carrigan et al. (2001) reported a summed probability age of ~352 Ma for ion microprobe zircon rims from the IP and eastern Blue Ridge. 342 Ma U–Pb ion microprobe age

records the growth of metamorphic zircon rims and coeval migmatite generation in intermediate and mafic metaigneous rocks in the Brindle Creek footwall near Lenoir, North Carolina (Kalbas et al., 2002; Bream, 2003). Robinson et al. (1998) proposed the term Neoacadian for a 366–355 Ma thermal event in New England, which has been adopted for the 360–345 Ma high temperature event in the southern Appalachians (e.g. Kohn, 2001; Hatcher, 2002). The 330–325 Ma ages are Alleghanian, recording the earliest thermal events connecting the Tugaloo, Cat Square, and Carolina terranes (Dennis and Wright, 1997a, b).

5. Detailed structure of the northern IP

New 1:12,000- and 1:24,000-scale detailed geologic mapping of 3740 km^2 in the northern IP has generated large amounts of data. These data create a new island of detailed geologic knowledge in the South Mountains-Columbus Promontory (SMC) (Fig. 5) and the Brushy Mountains (BM) (Fig. 6), and combined with existing islands of detailed data in the Carolinas and northeastern Georgia, form the basis for our 3-D analysis. Cross-sections constructed in a variety of orientations confirm that a 3-D deformation plan dominates the IP. Closely spaced serial sections constructed using down-plunge projections of detailed map geometries and mesofabric data provided the major first step toward 3-D analysis (Figs. 5 and 6).

The SMC island extends from the westernmost IP into the eastern IP. It contains the northeastern end of the ~490 Ma Henderson Gneiss and several Middle Ordovician–Silurian granitoids in the western IP, and Devonian to Carboniferous plutons in the eastern IP–Cat Square terrane. The Tumblebug Creek, Walhalla, and Six Mile-Sugarloaf Mountain faults are traceable from South Carolina into the SMC and terminate here. The Mill Spring fault is traceable from South Carolina through both the SMC and BM. The Mill Spring and Brindle Creek faults truncate footwall synclines that preserve Middle Ordovician Poor Mountain rocks (Fig. 5).

5.1. Superposition of structural elements in the northern IP

Early ductile Neoacadian to early Alleghanian structures are overprinted by later brittle deformation (late Alleghanian to Jurassic) (Table 1). These relationships are clearly resolved both in the mesofabrics, and geologic maps.

5.1.1. Foliation

Dominant foliation, S_2, in the IP wraps amphibolite and calc–silicate boudins that contain an earlier foliation (Hopson and Hatcher, 1988; Davis, 1993a; Bier et al., 2002; Merschat and Kalbas, 2002). This penetrative foliation consists of parallel orientation of phyllosilicate minerals, quartz ribbons, and other nonequant minerals, and is parallel to transposed compositional and new migmatitic layering. It is axial planar to F_2 ductile folds and folded by later ductile near (but probably post) thermal peak F_3 folds that locally develop an axial planar foliation (S_3). The foliation S_2 has a gentle to moderate dip throughout the northern IP (Figs. 2 and 7). Shear-sense indicators, including asymmetric tight folds, mesoscopic sheath folds, normals to axes of asymmetric boudins, S–C fabrics, and rotated porphyroclasts, taken together indicate the northern IP was deformed by heterogeneous simple shear (Davis et al., 1991). Mylonitic (C) foliation dominates in a 13–15-km-wide zone along the western flank of the IP that closely corresponds to domain I (Fig. 7) and locally in shear zones throughout the IP. All foliation components are annealed on the microscopic scale, except for some feldspar relicts and local subgrains that preserve later strain. Late coarse-grained, subhedral muscovite has overgrown the dominant foliation in sillimanite schist, generally at a high angle, and is locally parallel to the axial surfaces of later crenulations.

Dominant S_2 foliation is variously folded throughout the IP, but a systematic variation in orientation is present where abundant measurements exist in the SMC and BM (Fig. 7). A domain of strongly NE–SW-trending, gently to moderately SE-dipping foliation exists throughout the western IP and the leading edge of the Brindle Creek thrust sheet in the BM (Fig. 2). Less strongly aligned foliation domains exist to the east in both the SMC and BM. The weak axial-planar foliation developed in F_3 folds locally becomes a strong foliation near the Brindle Creek fault (Fig. 8a).

5.1.2. Lineations

An array of linear fabric elements formed in the IP, from mineral lineations to crenulations and other fold hinges, slickenlines, and intersections of the dominant foliation and compositional layering with later foliations (Table 1). The most commonly observed lineation in the IP is a mineral stretching lineation (L_2) composed of quartz, feldspar(s), and micas in quartzofeldspathic to granitic rocks; sillimanite and muscovite in pelitic rocks; and hornblende in intermediate to mafic rocks (Fig. 8b). This lineation was independently confirmed as a high temperature mineral stretching lineation by analysis of shear-sense indicators (asymmetric folds, sheath fold hinges, S–C fabrics, etc.) (Vauchez and Brunel, 1988; Davis et al., 1991; Davis, 1993a; Vauchez et al., 1993) and quartz slip systems (Davis, 1993a). It has a gentle plunge ($<15°$) and defines an

Fig. 5. Simplified detailed geologic map of the South Mountains–Columbus Promontory region modified from Bier et al. (2000). Data from Overstreet et al. (1963), Davis (1993a), Yanagihara (1994), Bream (1999), Giorgis (1999), Hill (1999), Williams (2000), and Bier (2001). Abbreviations: BCF—Brindle Creek fault; MSF—Mill Spring fault; SMF—Sugarloaf Mountain fault; TCF—Tumblebug Creek fault.

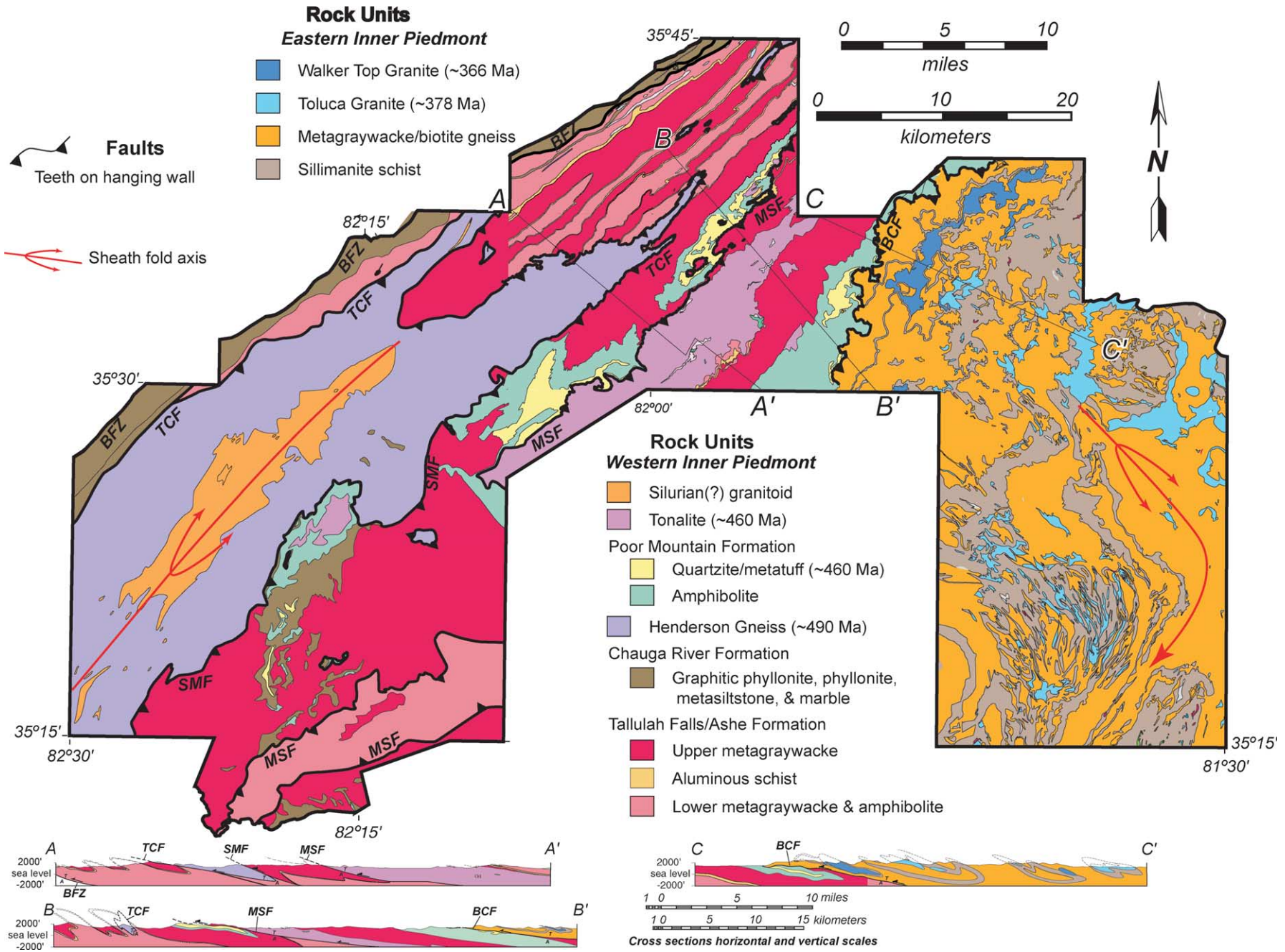
Rock Units
Eastern Inner Piedmont
Walker Top Granite (~366 Ma)
Toluca Granite (~378 Ma)
Metagraywacke/biotite gneiss
Sillimanite schist
Faults
Teeth on hanging wall
Sheath fold axis
0 5 10
miles
0 10 20
kilometers
N
35°45'
82°15'
35°30'
82°00'
35°15'
82°30'
82°15'
81°30'
BFZ
TCF
SMF
MSF
BCF
A
A'
B
B'
C
C'
Rock Units
Western Inner Piedmont
Silurian(?) granitoid
Tonalite (~460 Ma)
Poor Mountain Formation
Quartzite/metatuff (~460 Ma)
Amphibolite
Henderson Gneiss (~490 Ma)
Chauga River Formation
Graphitic phyllonite, phyllonite, metasiltstone, & marble
Tallulah Falls/Ashe Formation
Upper metagraywacke
Aluminous schist
Lower metagraywacke & amphibolite
2000'
sea level
-2000'
10 miles
15 kilometers
Cross sections horizontal and vertical scales

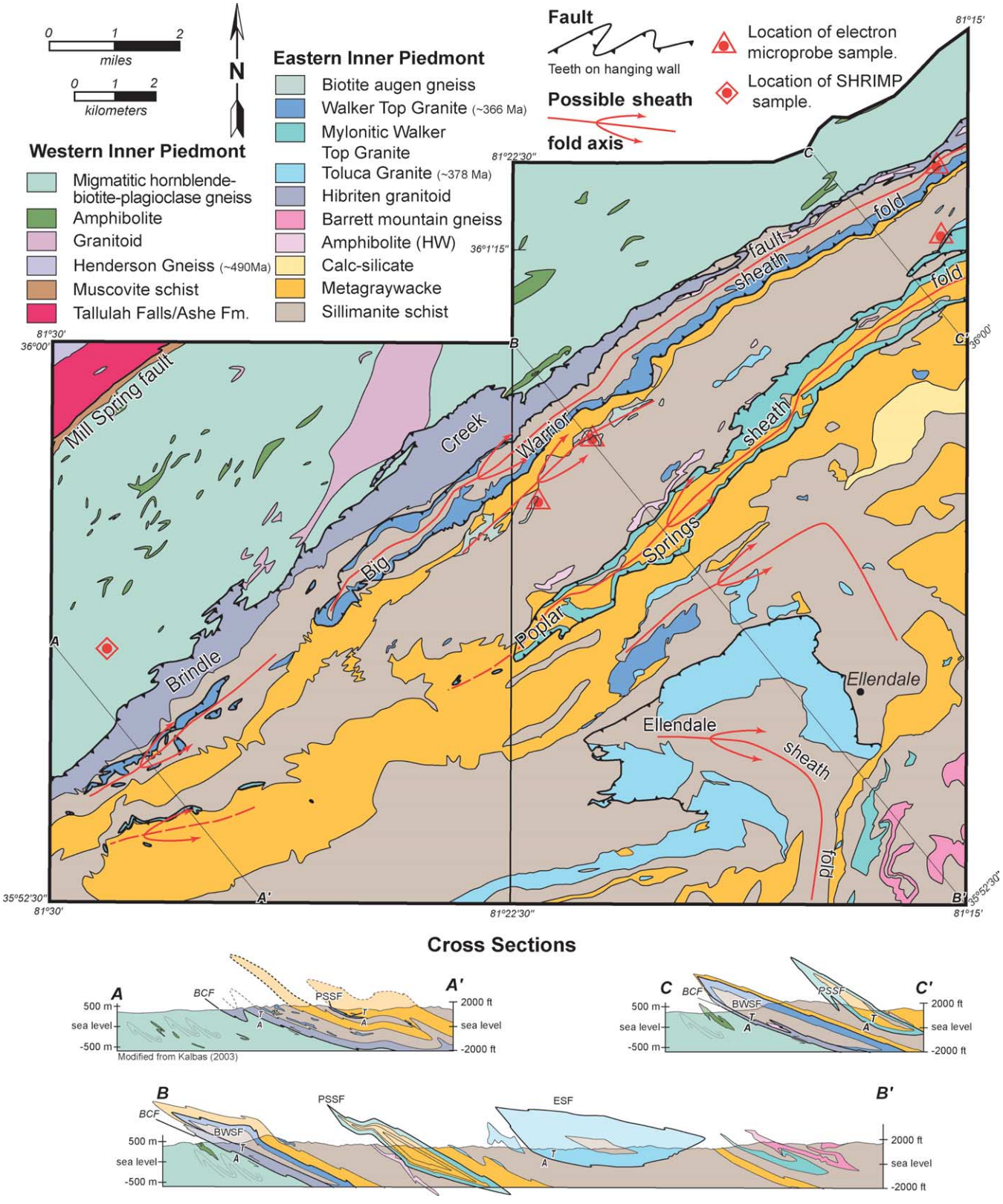

Fig. 6. Simplified detailed geologic map and cross-sections of the southwestern Brushy Mountains, North Carolina. Western part of map is from Kalbas (2003). BCF—Brindle Creek fault; BWSF—Big Warrior sheath fold; ESF—Ellendale sheath fold; PSSF—Poplar Springs sheath fold.

Table 1
Tectonic summary for the northern IP

EVENTS	STRUCTURES			METAMORPHIC CONDITIONS	REGIONAL EVENTS	OROGENY & TIMING
	Fabrics	Folds	Faults	Z PP Gs A G		
D_1	S_1 Early foliation preserved in amphibolite and calc-silicate boudins	F_1 Intrafolial folds and isoclinal folds preserved in boudins	———	M_1 Moderate to high pressure and temperature	Initial collision and subduction of IP beneath Carolina terrane	Pre- to early Acadian post ~410 Ma
D_2	S_2 Penetrative foliation L_2 Mineral lineation; curving pattern, trends NE-SW, E-W, & NW-SE	F_2 Inclined to recumbent, tight to isoclinal passive and flexural flow folds, and sheath folds; curving pattern trends NE-SW, E-W, & NW-SE	Initial NW and then SW deflected movement of IP faults	M_2 Peak metamorphism, upper amphibolite facies, sillimanite I & II grade	Continued subduction, emplacement of crystalline thrust sheets, and SW deflection along Neoacadian BFZ, channel flow	Neoacadian 360 – 345 Ma
D_3	S_3 Rare secondary foliation L_3 Mineral and intersection lineations	F_3 Inclined to upright, closed to open folds, trend NNE-SSW, N, & NW	Continued NW and SW movement on IP faults	M_3 Decreasing P-T conditions, high to moderate pressure and temperature	Initial subduction beneath Africa, final emplacement and exhumation of IP thrust sheets	Early Alleghanian 330 – 325 Ma
D_4	S-C and related fabrics in BFZ, & CPS Mineral lineations in BFZ, intersections in IP	F_4 Upright, open folds, trend NW-SE, & NE; crenulations plunge SE, & NE	Ductile reactivation of BFZ & CPS	Low pressure and temperature – greenschist facies (retrogressive)	Initial emplacement of the composite Blue Ridge-IP thrust sheet and exhumation	Alleghanian ~300 Ma
D_5	Joints Mineralized (?)	Regional broad, open folds, most trend NE & NW	Brittle movements associated with the Rosman fault of the BFZ	Brittle conditions	Continued emplacement and exhumation of the composite Blue Ridge-IP thrust sheet	Late Alleghanian ~260 Ma
$D_{6...}$	Filled joints Unfilled joints	Regional broad, open folds, trend NE	Meso- and macroscale normal faults	M_4 Brittle conditions	Rifting — ? — Uplift	Mesozoic extension — ? — Cenozoic uplift

Shaded curve under metamorphic conditions represents changes in P–T conditions, identifying peak conditions in each event. Metamorphic facies: Z—Zeolite; PP—Prehnite–Pumpellyite; Gs—Greenschist; A—Amphibolite; G—Granulite; BFZ—Brevard fault zone; CPS—central Piedmont suture.

asymmetric pattern of very strong NE–SW alignment to the northwest (domain I, Fig. 7) and a curved pattern across the IP (Fig. 2b). This pattern has been reconfirmed where more detailed data exist, e.g. in the SMC, BM (Fig. 7a), and elsewhere in the IP (e.g. Grant, 1958). Reed and Bryant (1964) collected mineral lineation data in the western IP and quartz c-axis data in the BFZ and first suggested the BFZ is a dextral fault, but they included coaxial high temperature and retrograde lineations that formed during two separable dextral phases of BFZ movement in their analysis.

5.1.3. Folds

The earliest folds are rare tight-to-isoclinal passive to flexural flow folds (F_1) that occur in boudins and as intrafolial folds, which are wrapped and transposed by the dominant S_2 foliation (Table 1). These were superposed by F_2 tight-to-isoclinal and sheath folds that formed coevally with the axial planar S_2 foliation and the coaxial L_2 mineral stretching lineation. Axial surfaces commonly have shallow to moderate dip, and axial trends mimic the lineation pattern (Fig. 7). Relatively few mesoscopic sheath folds have been observed in the field (Fig. 8c and d), possibly because many of the mesoscopic F_2 folds measured in small exposures may comprise one limb of larger mesoscopic sheath folds, again suggesting very high finite strain.

Post-metamorphic peak F_3 flexural flow folds fold the S_2 foliation (and compositional layering), and only locally develop an axial-planar S_3 foliation (Table 1; Fig. 8a). These folds mostly trend NE–SW, have axial surfaces that dip moderately SE, plunge gently NE or SW, and verge NW. They coaxially superposed F_2 folds in the strongly aligned part of the IP, but cross F_2 folds at a high angle farther SE. F_3 folds probably formed during a similar deformation event as F_2 folds. The strong coaxial alignment of F_2 and F_3 folds in the western IP may be kinematically linked to the later stages of D_2. F_3 folds do, however, fold the major faults in both the SMC and BM (Figs. 5 and 6), additionally delimiting the timing of the large faults.

Multiply trending and verging crenulation folds superpose all earlier structures, and are most common in

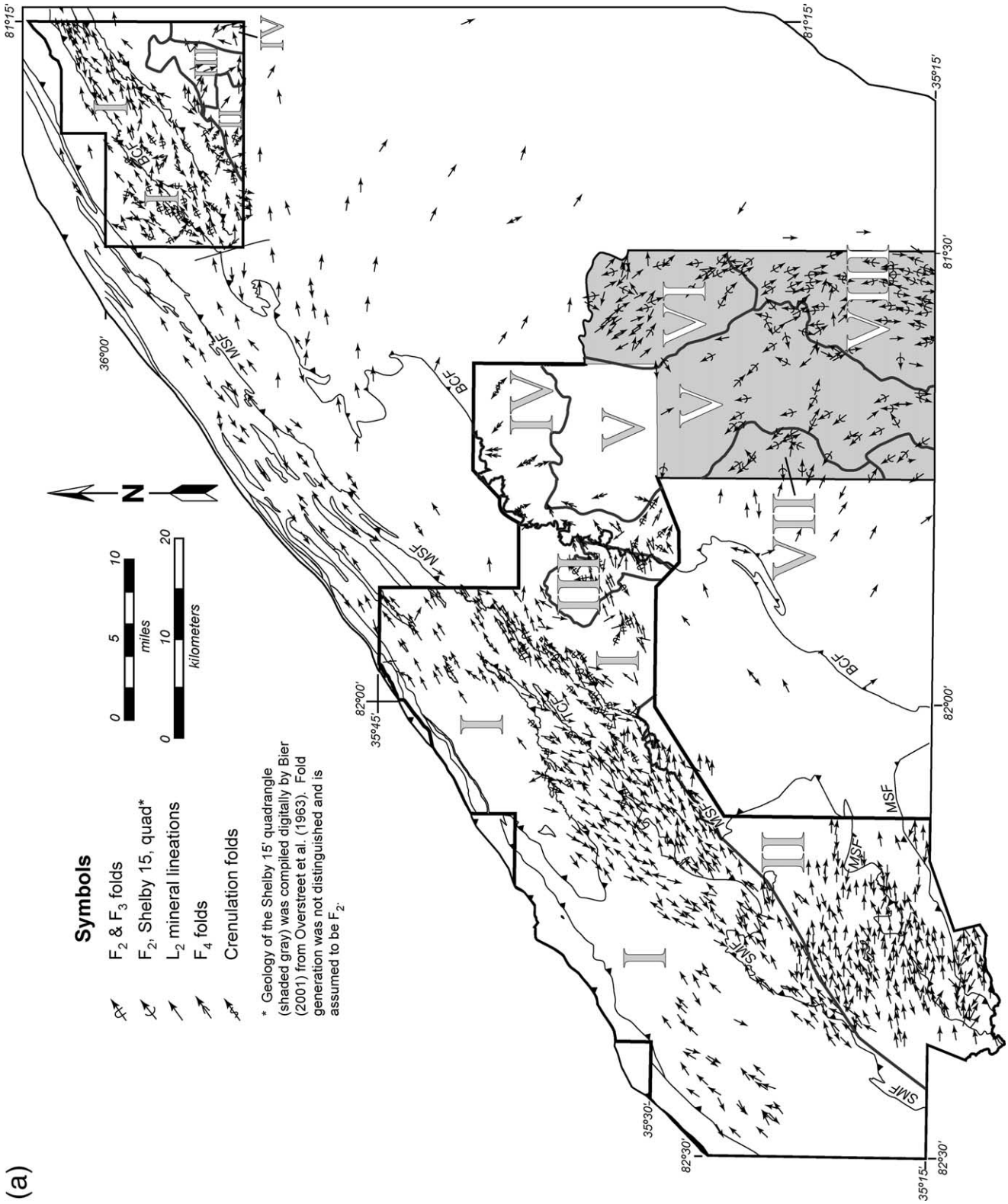
(a)
Symbols
F2 & F3 folds
F2, Shelby 15, quad*
L2 mineral lineations
F4 folds
Crenulation folds
* Geology of the Shelby 15' quadrangle (shaded gray) was compiled digitally by Bier (2001) from Overstreet et al. (1963). Fold generation was not distinguished and is assumed to be F2.
N
0 5 10 miles
0 10 20 kilometers
81°15'
36°00'
35°45'
35°30'
35°15'
82°00'
82°30'
81°30'
BCF
MSF
SMF
I
II
III
IV
V
VI
VII
VIII

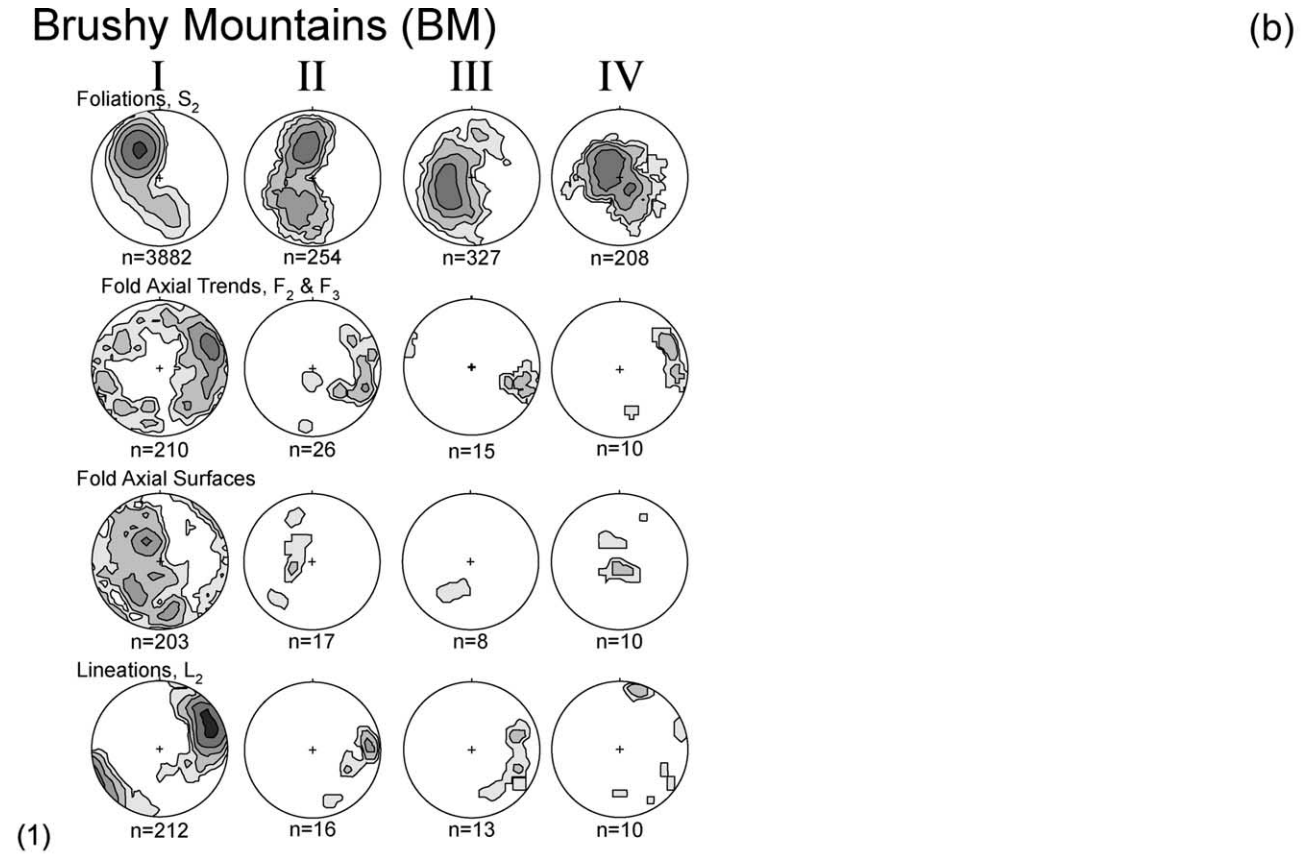

Fig. 7 (*continued*)

mica-rich interlayers and the sillimanite schist map unit (Table 1; Figs. 7a and 8e). Later upright mostly NW–SE-oriented open (brittle), gently plunging flexural-slip folds occur throughout the IP. Although none of these folds developed a prominent axial-planar cleavage, the F_5 crenulation cleavage could be related to tightened flexural-slip folds or open F_3 folds that were never tightened.

5.1.4. Other structures

A range of high to low temperature deformed to undeformed quartz–feldspar pegmatite, quartz–epidote–calcite, chlorite–quartz, quartz, and zeolite–prehnite–calcite veins, and unfilled joints exist in the IP indicating brittle deformation occurred from the time decompression melting would have affected the rocks through various stages of late Paleozoic to Mesozoic and Cenozoic fracture formation. A suite of steeply dipping, near E–W-trending coeval Jurassic faults and NW-trending diabase dikes occurs in the IP along the North Carolina–South Carolina border (Garihan et al., 1990, 1993). Similar faults and NW-trending diabase dikes occur in the topographic low separating the South and Brushy Mountains. These faults are characterized by multiple reactivation and fillings of vuggy siliceous cataclasite.

5.2. Timing of deformation

Early ductile deformations in the IP are bracketed by Paleozoic detrital zircons, Devonian intrusions, and timing of peak metamorphism. Rare D_1 structures postdate ~430 Ma detrital zircons from the Cat Square terrane, and are probably closely related to intrusion of the ~378 Ma Toluca Granite. Later D_2–D_3 ductile deformations postdate intrusion of the penetratively deformed 366 Ma Walker Top Granite. Coplanar relationships between S_2, migmatitic layering, and F_2 axial surfaces, and coaxial relationships of L_2 and F_2 suggest D_2 produced the majority of near thermal peak micro-to-macroscopic structures in the IP between 360 and 345 Ma. Documented F_2 folds superposed by locally near-coaxial ductile F_3 folds suggest D_3, at 330–325 Ma, was similar to D_2, but not as extensive.

6. Macroscopic sheath folds

Mesoscopic sheath folds occur in all thrust sheets in the northern IP (Davis, 1993a; Yanagihara, 1993; Williams, 2000; Bier et al., 2002) (Fig. 8c and d). Sheath fold axes, axes of early, tight to isoclinal mesoscopic folds and mineral lineations are coaxial throughout the IP. Sheath fold axes lie in S_2, supporting the interpretation that S_2 is mostly a C foliation.

Map patterns in the northern IP (Figs. 5 and 6) are typical of patterns reported elsewhere for sheath folds (Cobbold and Quinquis, 1981; Alsop and Holdsworth, 1999, 2002; Azcárraga et al., 2002). Davis (1993a), Bream (1999), and Hatcher (2002) have suggested the ~490 Ma Henderson Gneiss body in the western IP occupies a map-scale sheath fold based on map pattern, penetrative mylonitic fabric, consistent top-to-the-SW shear sense indicators, and map patterns and mesofabrics at its southern termination (Figs. 2 and 9). The outliers of Henderson Gneiss northeast of the main intact body are interpreted as synformal sheath folds (Hatcher, 2002) (Fig. 10b). In the SMC the Henderson Gneiss reaches its greatest outcrop width and its map pattern might be explained simply as a penetratively deformed pluton (Fig. 5), but the southern termination is more complex (Fig. 9). Here oppositely verging, asymmetric folds extend southwestward from the main body and converge to form the apex of an imbricated SW-verging sheath fold. Sheath fold axes plunge between 0° and 15° NE, parallel to the length of the main Henderson Gneiss body, mineral lineations, and mesoscopic fold axes in the strongly aligned domain in the western IP (Figs. 2, 5 and 7).

Bier (2001) and Bier et al. (2002) interpreted domains III–VII (Figs. 5 and 7) as parts of a SE-plunging map-scale sheath fold. This interpretation was based on cross-section geometry, and orientation of mineral lineations and fold axes symmetrically about the tongue-shaped map pattern (Bier, 2001; Bier et al., 2002). The Walker Top Granite occupies the core of this sheath fold based on the Walker Top Granite outcrop pattern near the trace of the Brindle Creek fault. Furthermore, the map pattern and related mesofabrics indicate similarly oriented macroscopic sheath folds occur in the southeastern part of Fig. 5.

Disconnected map-scale pods (boudins?) and linear bands of nonmylonitic and mylonitic Walker Top Granite outline linear NE-plunging sheath folds in the BM (Fig. 6). The northwestern band of Walker Top Granite outlines the limbs of the Big Warrior sheath fold. The hinge of the southern Poplar Springs sheath fold extends southwest of the BM. Mineral lineations and mesoscopic fold axes in domain I parallel sheath fold axes. Disconnected bodies of Toluca Granite in the southeastern part of the map (Figs. 6 and 7, domains II–IV) comprise the curved WSW-directed Ellendale sheath fold. The sheath axis curves through a 130° arc with parallel changes in mineral lineation and mesoscopic F_2 fold axis orientation. Mesoscopic folds on opposite limbs of the sheath folds verge NW and NE on the north limb and SW on the south limb, as predicted by

Fig. 7. (a) Homogeneous domains based on trends of the dominant foliation of the (1) BM and (2) SMC. Mineral lineations and folds axes are shown to illustrate curved lineation pattern in the SMC and BM. SMC domains IV–VIII were compiled by Bier (2001) and Bier et al. (2002). Folds compiled from that area in the SE part of the map were assumed to be F_2. (b) Contoured lower-hemisphere, equal-area plots of poles to foliation, and trends of fold axes and mineral lineations for the domains defined in (a). Folds plotted include only passive and flexural flow F_2 and F_3 folds. Contours 1, 2, 4, 8, and 16% per one percent area. Data in SMC domain II from Davis (1993a,b). Axial surfaces were not measured in all folds and were not available in domains IV–VIII in the SMC.

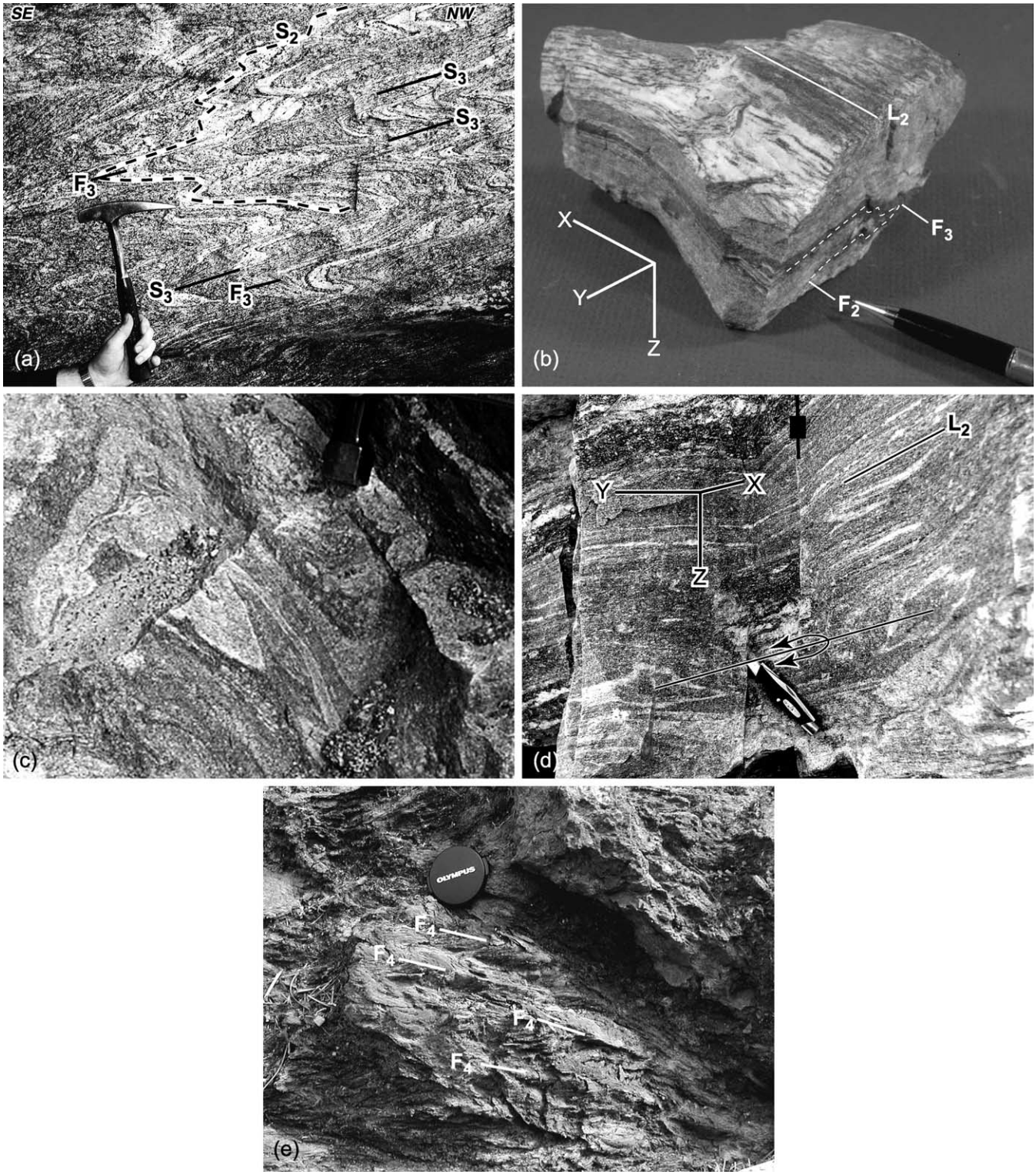

Fig. 8. (a) Development of rare S_3, axial planar to reclined, isoclinal passive flow folds, F_3, in quartz–hornblende–plagioclase migmatite (Poor Mountain Amphibolite protolith?) in the footwall of the Brindle Creek fault in the BM. F_3 fold axes plunge gently NE and verge NW. Orientation of photo is NW to the right. Located NE of Lenoir, North Carolina, in the SE corner of the Kings Creek quadrangle. (b) L_2 mineral lineation defined by hornblende and rodded quartz parallel to F_2 isoclinal fold axes, which here are coaxially refolded by F_3 inclined asymmetric folds. Sample from Middle Ordovician Poor Mountain felsic tuff and amphibolite from NE of Toccoa, Georgia, in the SW part of the Tugaloo Lake quadrangle. (c) Anvil-shaped sheath fold (*YZ* section) in migmatitic metagraywacke/biotite gneiss of the Brindle Creek thrust sheet from the Morganton Quarry, Morganton, NC. Tip of hammer head in upper right-hand corner indicates scale. (d) Eye-shaped sheath fold in mylonitic Walker Top of the northwest limb of the Poplar Springs sheath fold in the 115 Quarry, Wilkesboro, NC. Sheath fold is exposed on two surfaces, a horizontal (left) and near vertical surface (right). Sheath fold axis, 22°, N 54° E, is parallel to the L_2, and within S_2. Sheath fold verges SW. Pocket knife is 7.4 cm long. (e) ESE-trending F_4 crenulations in sillimanite–schist of the Brindle Creek thrust sheet from U.S. 64 in the southern Ellendale quadrangle, North Carolina. Lens cap diameter is 4.3 cm.

Alsop and Holdsworth (1999, 2002) for 3-D sheath folds in Scotland.

Several geometric differences, largely predicted by location, exist between map-scale sheath folds in the IP. The Henderson Gneiss cores a series of large NE-plunging flattened tubular sheath folds in the westernmost IP. Eastern IP sheath folds are defined by bands and map-scale granitoid boudins that outline the folds (Fig. 6), probably the result of contrasting strengths of the stronger granitoids and surrounding weaker schist, similar to experimental models of Cobbold and Quinquis (1981). Walker Top Granite sills(?) have been deformed and outline NE-plunging tubular sheath folds in the western part of the Brindle Creek thrust sheet in the BM. The curved Ellendale sheath fold in the southeast corner of Fig. 6 is much less strained and transposed than those farther northwest. As a result, it is not tubular except at the hinge and retains a more anvil-shaped cross-section to the southeast.

Location of the Toluca and Henderson granitoids in the cores versus limbs of sheath folds may be related to the original geometry of the granitoid. The Henderson Gneiss probably is a deformed batholith (Fig. 10), whereas the eastern IP granitoid bodies are much smaller and may have been tabular plutons transposed into tubular sheath folds (Fig. 11).

7. Kinematics and 3-D deformation plan

7.1. Crustal flow

Sheath folds, contrasting structural domains, mineral lineation patterns, and shear-sense indicators are all important elements in understanding the 3-D deformation plan of the northern IP. Tectonic transport parallel to sheath folds is well documented elsewhere (Quinquis et al., 1978; Cobbold and Quinquis, 1981; Alsop and Holdsworth, 1999, 2002; Azcárraga et al., 2002). L_2 mineral lineations are synkinematic and parallel to both map- and mesoscale sheath fold axes. Sheath folds developed as a product of noncoaxial ductile flow at mid-crustal depths, 15–20 km, at near-peak upper amphibolite facies metamorphic conditions (Bier et al., 2002; Merschat and Kalbas, 2002).

IP flow paths thus parallel sheath fold axes, and are tracked by the lineation pattern permitting formulation of a 3-D kinematic model for the IP (Fig. 12), anticlockwise flow across the IP. To the east, flow is dominantly N- and NW-directed, and changes to W-directed flow near the axis of the IP (Fig. 12). Along the western flank, W-directed flow is deflected SW in a 13–15-km-wide zone of constricted flow related to buttressing against the rock mass northwest of the Neoacadian BFZ (Davis, 1993a; Hatcher, 2001; domain I, Fig. 7). In the BM the northwestward change from N- and NW- to SW-directed flow is more abrupt and the only area of W-directed flow is in domain II (Figs. 7 and 12). The change is gradual in the SMC, where a broader area of W-directed flow exists (Fig. 12). It is likely that SW-directed stretching and vertical thinning occurred here, similar to model E of Fossen and Tikoff (1998), and consistent with the conclusions of Dewey et al. (1998).

Our 3-D kinematic model for the northern IP thus involves dextral transpression and curving noncoaxial ductile flow during the Neoacadian tectonothermal event (Fig. 13). Oblique collision of the Carolina terrane and A-subduction of the IP (and eastern Blue Ridge?) led to deep burial, mid-crustal P–T conditions, and inhomogeneous thrusting and plastic flow. The Smith River allochthon (Fig. 1a), lying north and west of the Sauratown Mountains window and the IP, appears to be an outlier of the Carolina terrane (Hibbard et al., 2002, 2003), and not a remnant of an IP thrust sheet as suggested previously (e.g. Hatcher, 1989). If so, this supports the hypothesis that the Carolina terrane has overridden the IP, and the Neoacadian BFZ marks the SW-directed escape of high-grade IP rocks.

7.2. Faults and flow kinematics

Understanding the 3-D kinematic history of northern IP faults requires integration of all available structural data with the 3-D flow model. Faults in the Neoacadian BFZ are characterized by NE–SW-trending subhorizontal mineral lineations that are sub-parallel to fault traces. Shear-sense indicators associated with the Tumblebug Creek fault (Davis, 1993a,b), Sugarloaf Mountain fault (Davis, 1993a, b; Bream, 1999), and Poplar Springs sheath fold yield consistent top-to-the-SW shear sense, and therefore have significant dextral motion.

Faults traced across flow gradients have varied geometries and kinematics related to the respective flow regime in which they occur. The Mill Spring and Brindle Creek faults both cross flow gradients from the southwestern SMC to the BM. Based on W-verging macroscopic folds and top-to-the-W shear sense in the SMC, Davis (1993a,b) suggested that the Mill Spring fault is a gently dipping ($<10°$) W-directed thrust located in the eastern flow domain. Northward the fault occurs in the Neoacadian BFZ, lineations parallel the NE–SW trace of the fault and the dip increases (30° or more). Muscovite fish, asymmetric porphyroclasts, in concert with down-dip plunge of intersections of S and C planes yield top-to-the-SW shear sense, consistent with SW-directed flow of the Neoacadian BFZ. Similar relationships occur along the Brindle Creek fault. In the SMC the Brindle Creek fault is located east of the strongly SW-directed zone of constricted flow and appears to have dominant W-directed motion here based on its E–W-trending mineral lineation, and W- to NW-vergent meso- and macroscopic folds (Giorgis, 1999; Williams, 2000; Bier et al., 2002). Farther north near Morganton, NC, and northeastward into the BM, the kinematics of the Brindle Creek fault change (Figs. 7 and 12): the fault, together with some 5 km of its hanging wall (at the present erosion level), are caught up in the SW-directed zone of constricted flow in the Neoacadian BFZ (Fig. 12). The strongly SW-vergent Big Warrior and

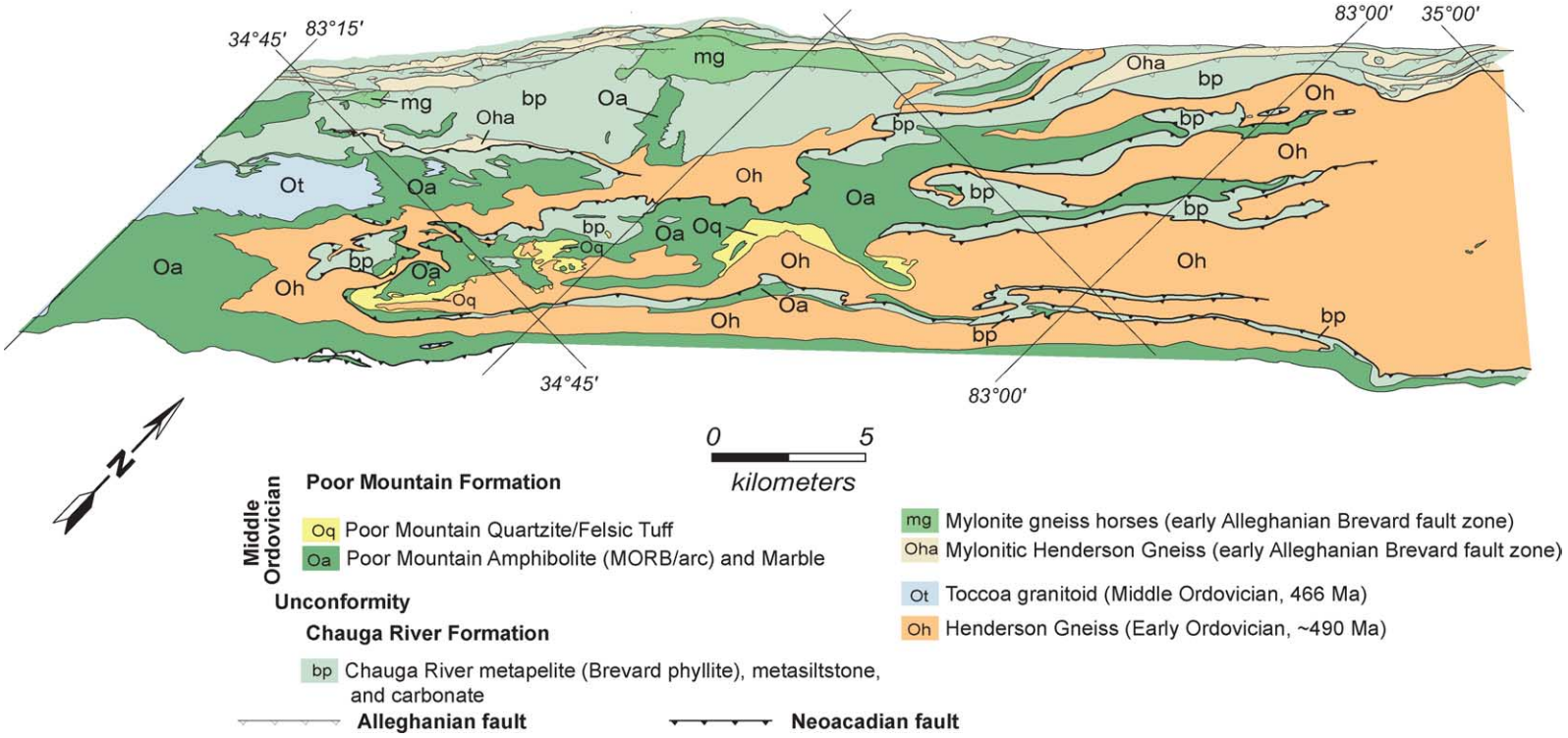

Fig. 9. Henderson Gneiss and Poor Mountain Formation rocks repeated on SW-directed sheath fold thrust imbricates at the southwest end of the Henderson Gneiss body in South Carolina. Note that there is an early set of thrusts (with smaller solid teeth), and a later set (with larger open teeth) confined to the BFZ. Although the early faults have map configurations of low-angle thrusts, shear-sense indicators and shallow plunge and strong NE orientation of L_2 indicate the thrusts moved SW. Apparent NW-verging early plastic (isoclinal-recumbent) folds are probably components of the NW limbs of SW-directed sheath folds. Compiled and modified from detailed geologic maps from Griffin (1973, 1974b), Hatcher and Acker (1984), Hatcher (unpublished data), and Hatcher and Acker (unpublished data).

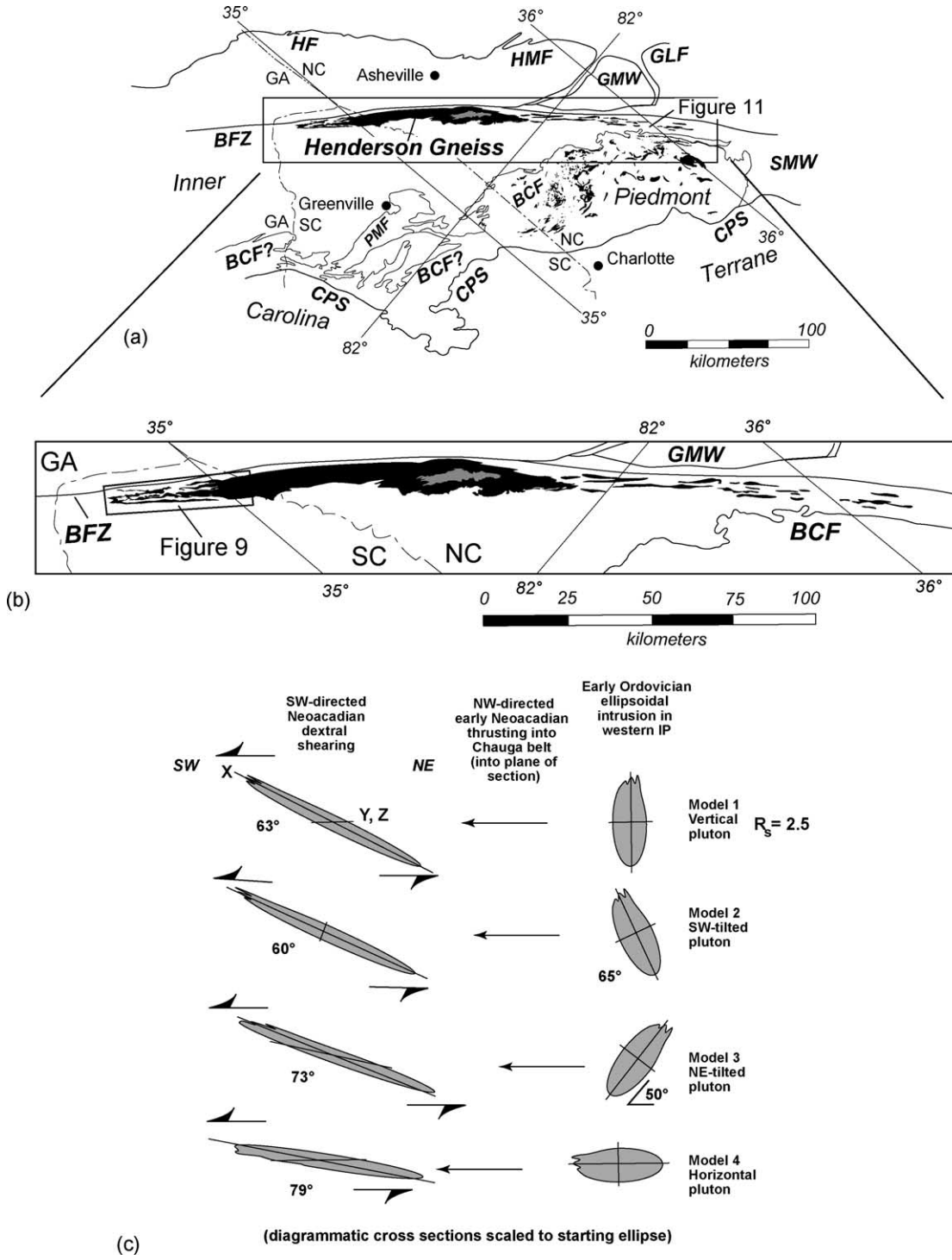

Fig. 10. Bulk strain estimates for Henderson Gneiss. (a) Locations of Henderson Gneiss in the western IP, and Walker Top and Toluca Granite bodies in the eastern IP (small abundant black bodies in the northern Brindle Creek thrust sheet). Note that the relative size of the Henderson Gneiss dwarfs that of the Walker Top and Toluca bodies. Abbreviations are the same as in Fig. 1. (b) Outcrop pattern of the Henderson Gneiss (black). Gray body inside Henderson Gneiss is an unnamed Silurian granitoid. (c) Four possible models for SW-directed shear deformation of the Henderson Gneiss batholith, assuming it had an initially ellipsoidal shape and an R_s (initial ellipticity) of 2.5, which produce approximately the same length body as the present main Henderson Gneiss body.

Poplar Springs sheath folds and the NW part of the Ellendale sheath fold in the BM (southeast corner of Fig. 6) record this transition in the Brindle Creek hanging wall from NW- and W-vergent structures to the east to strongly aligned, SW-vergent structures to the west. Location of the transition zone between flow regimes, from NW- and W-directed flow to SW-directed flow, is possibly an erosional artifact of unroofing of this part of the orogen, but possibly

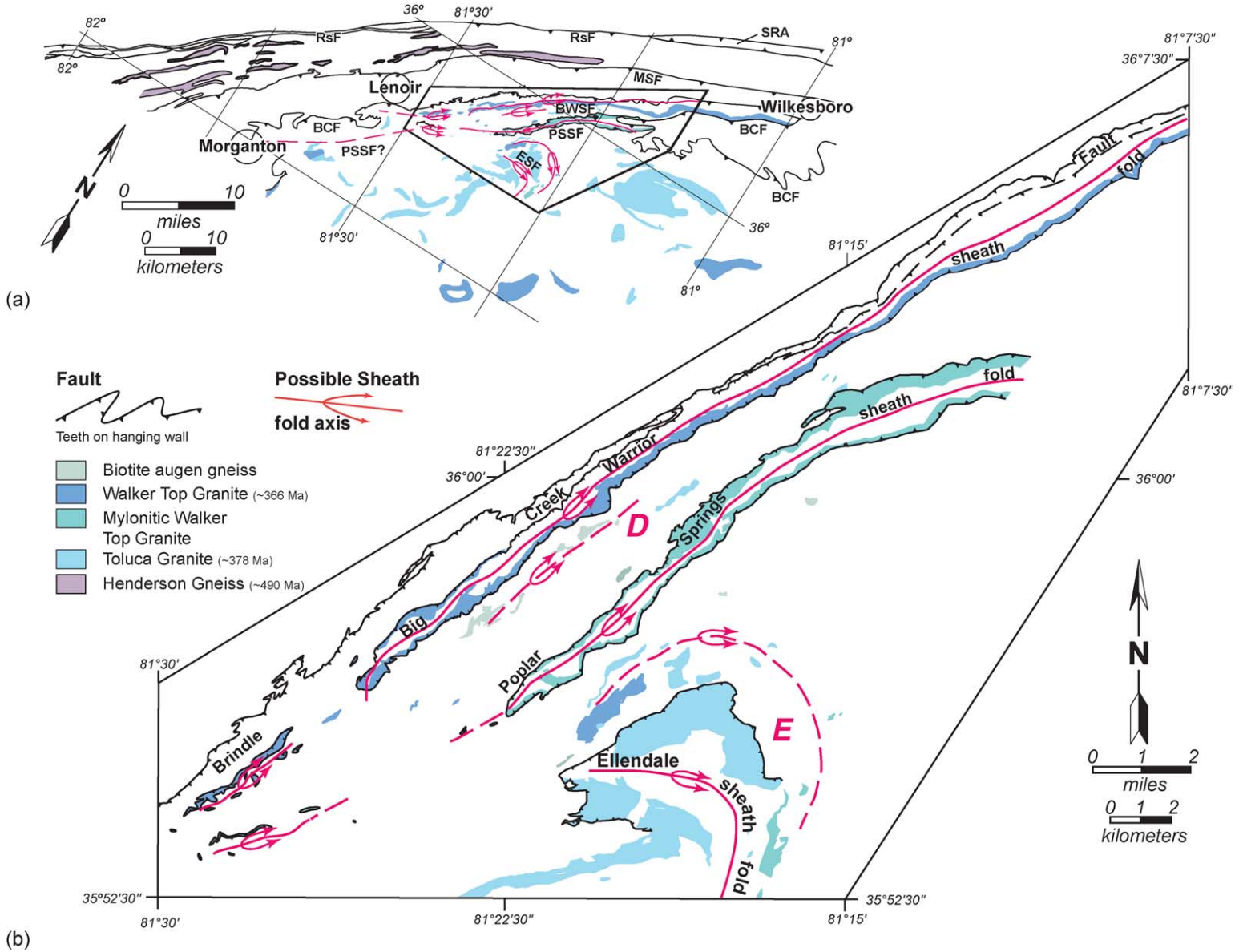

Fig. 11. Simplified geologic maps of (a) northwestern IP and (b) part of the SW BM showing structures in the Brindle Creek fault hanging wall and Walker Top and Toluca Granite bodies dismembered by SW-thrusted sheath folds. BCF—Brindle Creek fault; BWSF—Big Warrior sheath fold; ESF—Ellendale sheath fold; MSF—Mill Spring fault; PSSF—Poplar Springs sheath fold; RsF—Rosman fault; SRA—Smith River allochthon.

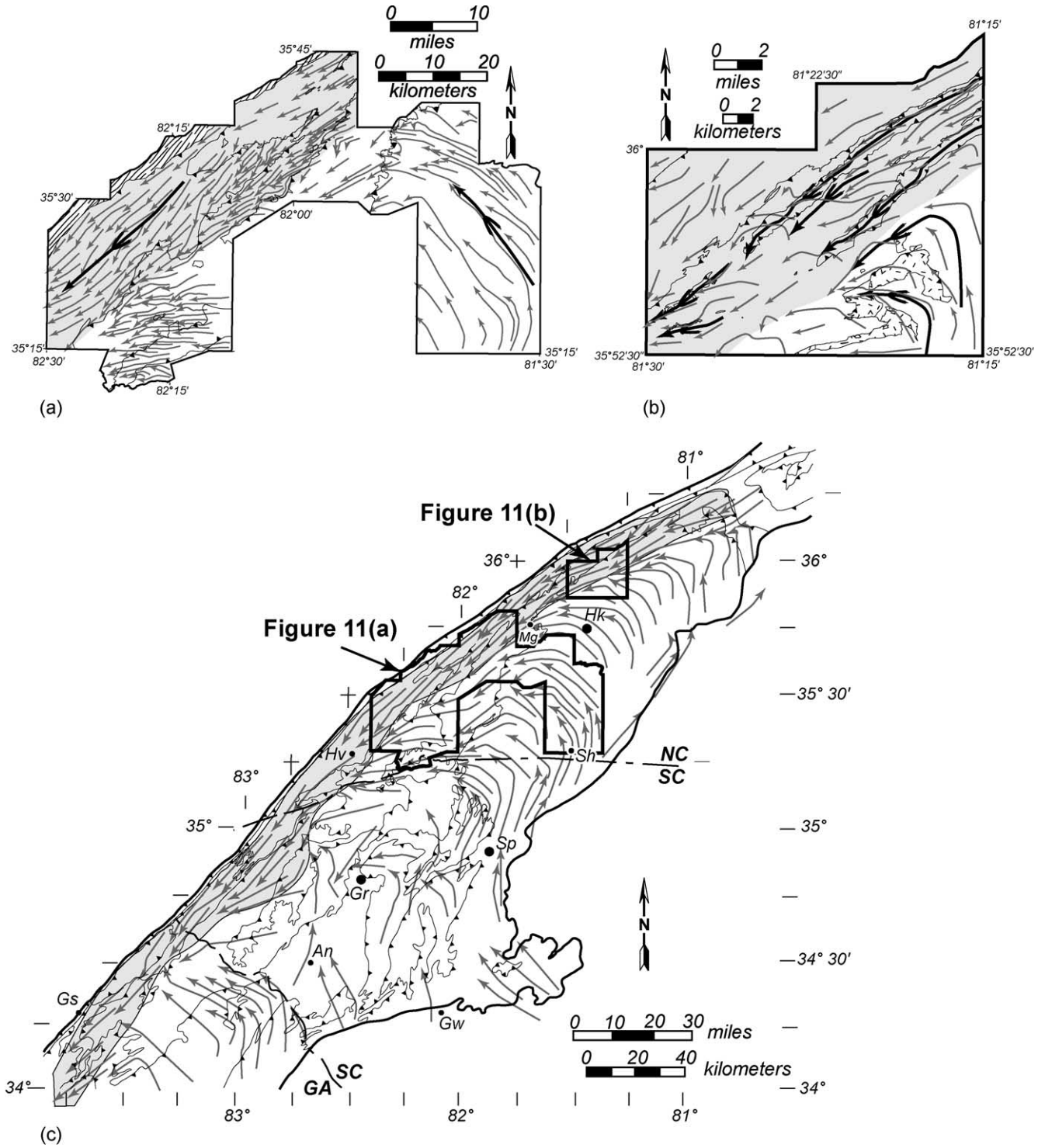

Fig. 12. Flow paths constructed from mineral lineations (thin dark gray arrows) and sheath fold axes (heavy black lines) for the (a) SMC, (b) BM, and (c) northern IP. Zone of strong alignment and constricted flow in the Neoacadian BFZ is highlighted in gray.

also related to fault displacement. Kinematics of IP faults are dictated by the transpressional crustal flow regime driven by the oblique collision of the Carolina terrane against the obliquely oriented Blue Ridge buttress, A-subduction of the IP, and possible SW-directed channel flow.

8. Estimates of bulk strain and fault displacement

The IP undoubtedly records large amounts of high temperature internal strain coeval with crystalline thrust sheet emplacement. Many rock bodies, such as homogeneous equigranular granitoids (e.g. Dysartsville Tonalite,


Eastern IP
Walker Top Granite
Toluca & Cherryville Granites
Sillimanite schist
Metagraywacke
Amphibolite
Biotite-amphibole gneiss
Hibriten mylonite
Cat Square terrane
Western IP
Henderson gneiss
Mill Spring thrust sheet
Marion thrust sheet
Brevard fault zone
Sauratown Mountains window
Tugaloo terrane
Smith River allochthon
Carolina terrane
Carolina terrane
Figure 13b
(a)
(b)
WS
SMW
BoCF
RF
MSF
BCF
SRA
ct
cps
Wk
RSF
BGF
Hk
Ln
Mg
MF
Sh
Hv
Oh
20 km
0
4,000 ft
1 km
BMSF
pSSF
ESF
Present erosional surface

Toluca Granite), do not readily yield shear sense information, whereas others, such as highly deformed megacrystic granitoids (Henderson and Walker Top Granites), provide useful shear-sense data. Metagraywackes (biotite gneisses) provide information on shear sense where they contain good markers (e.g. asymmetric folds, rotated porphyroclasts) but, where they have uniform texture, they reveal mostly static recrystallization and an annealed microfabric, while pelitic interlayers and mappable aluminous schist units record a strong S–C fabric that yields shear-sense data. This information, coupled with quartz c-axis data from the western IP (Davis, 1993b), confirm major fault displacement field and crustal flow regime that is well depicted by the regional high temperature lineation pattern.

Quartz and mica microfabrics in IP rocks, except those in or near Mesozoic fault zones and along the late brittle Rosman fault in the Brevard fault zone (Hatcher, 2001), are largely dynamically to statically annealed by available thermal energy accompanying deformation at near peak metamorphic conditions. Quartz c-axis fabrics, where they have been determined (Vauchez and Brunel, 1988; Davis, 1993a), *do* yield useful information from a variety of lithologies, but they have not been determined either over a large area or by systematic traverses across most of the IP. Because of this we have attempted to estimate bulk strain for parts of the northern IP using mesoscopic to map-scale structures.

8.1. Deformed granitoids and sheath folds

Several IP granitoids at the present erosion level are stocks and batholiths. Present map-scale geometries of these granitoids reflect Neoacadian ductile deformation that partially dismembered the Walker Top and Toluca plutons (Fig. 11) and markedly distorted the original Henderson Gneiss pluton shape (Figs. 9 and 10). There probably are numerous other map-scale sheath folds in the IP (e.g. Fig. 5), but either the detail of geologic mapping is not sufficient to resolve these structures or map-scale strain markers are absent.

Distorted and dismembered pluton geometries may be used to estimate local minimum bulk strain where they occur in the IP, but several assumptions must be made. (1) All strain recorded by the granitoids accumulated in one Neoacadian event, justified by dominance of Neoacadian metamorphic ages and lack of evidence of older metamorphism (e.g. Dennis and Wright, 1997a; Kalbas et al., 2002; Bream, 2003). (2) Geometries of deformed granitoids used here are well mapped. (3) Initial shapes can be approximated by ellipsoidal (Henderson) or tabular (Walker Top, Toluca) shapes, with the caveat that these are catazonal plutons, which may have had very irregular initial shapes. (4) Deformation was isovolumetric.

The Henderson Gneiss is areally the largest pluton in the southern Appalachians (Figs. 1, 9 and 10). We here consider it a large originally ellipsoidal strain marker, with several possible initial orientations. It consists of a main body that is imbricated at its southwest end by SW-directed thrusts and sheath folds (Fig. 9) and has numerous satellite outliers to the northeast (Fig. 10b). The mesofabric and associated consistently SW-directed shear-sense indicators (S–C fabric, rotated porphyroclasts, mineral elongation lineation) throughout the Henderson Gneiss body (Fig. 3) indicate that it is thoroughly internally deformed with k values (from deformed porphyroclasts) ranging from $k=1$–3 in most of the body to $k=3$–5 at the southwestern end, and $k=12$–15 in local high strain zones. If the dimensions of the intact portion of the Henderson Gneiss (110 km long, 12 km wide, estimated 6 km thick) measure minimum strain and an assumed initially ellipsoidal shape with initial ellipticity $R_s=2.5$ (dimensions: 50 km long, 20 km wide and thick), numerous alternative initial orientations exist to which SW-directed shear strain could be applied. We consider only four possibilities in cross-section here for the long axis of the pluton: vertical, tilted southwest, tilted northeast, and horizontal (Fig. 10c). In order to deform the initial ellipsoid configurations into bodies about 110 km long, the initial shapes must be sheared through angles of 63, 60, 73, and 79°, respectively. The ellipsoid with initial northeast tilt (Model 3) would first have undergone long-axis shortening, followed by elongation; all other ellipsoids would have undergone only progressive long-axis extension. Elongation of the long axis would be roughly 200% (~50 km) using this assumed initial ellipsoidal configuration. If the partially dismembered imbricates at the southwest end of the Henderson body are added to the intact body an additional 30 km extension parallel to the X-axis is 280% (~80 km elongation). If the entire outcrop length encompassing all Henderson Gneiss bodies, ~190 km, is assumed to be its total X-axis distribution (and the outliers synformal sheath fold hinges of a large intact sheath fold that includes all of the Henderson Gneiss), extension parallel to the X-axis is 486% (190 km extension). This analysis could be repeated employing a totally different set of assumptions and

Fig. 13. (a) 3-D block diagram depicting the structure of part of the northern IP from near Hendersonville, NC to the Sauratown Mountains window. Trend lines on the surface of the block were drawn from mineral lineations. Inset diagram shows location of map-scale sheath folds. Vertical exaggeration 1.3:1:1 (X:Y:Z). BCF—Brindle Creek fault; BoCF—Bowens Creek fault; cps—Central Piedmont suture; ct—Carolina terrane; MSF—Mill Spring fault; MF—Marion fault; Oh—Henderson Gneiss; RF—Ridgeway fault; RsF—Rosman fault; SMW—Sauratown Mountains window; SRA—Smith River allochthon. Towns: Hk—Hickory; Hv—Hendersonville; Ln—Lenoir; Mg—Morganton; Sh—Shelby; Wk—Wilkesboro; WS—Winston-Salem. (b) 3-D block diagram of part of the BM from the Brindle Creek fault to the Ellendale sheath fold. Trends on block surface drawn from lineations; form lines in cross-sections indicate dip of foliation. No vertical exaggeration, but the projection makes dip appear steeper. BCF—Brindle Creek fault; BWSF—Big Warrior sheath fold; ESF—Ellendale sheath fold; PSSF—Poplar Springs sheath fold.

parameters, yielding different results, but our purpose here is to construct a reasonable model based on reasonable assumptions to explore the range of internal strain and shape change of the Henderson Gneiss batholith.

The dismembered Walker Top and distorted Toluca Granite bodies in the southwestern BM (Figs. 6 and 11), because of their present outcrop patterns, are assumed to have had an originally tabular rather than elliptical shape. This is likely an oversimplification because these, like the Henderson Gneiss, are catazonal plutons that likely never had a classic 'tabular' shape. Using this assumption, an estimate of minimum axial elongation in the transport direction might be obtained by estimating the initial length of each deformed pluton, then measuring the separation between outliers. A potential flaw in this assumption is the possibility that the bodies are actually connected at depth and the mapped dismembered configuration is an artifact of the present erosion level. The assumption that these segments were separated from an original intact tabular pluton, however, is consistent with other data on SW-directed ductile fault transport and crustal flow. The Big Warrior sheath fold (Fig. 11) consists of a very linear body of mylonitic and nonmylonitic Walker Top Granite that has a northwestern limb preserved for only about 15% of its outcrop length. This northwestern segment was excised to the northeast by the Brindle Creek fault (Fig. 6). Toward the southwest along strike are numerous outliers of Walker Top Granite interpreted to be dismembered segments of the previously continuous pluton. The distance from the southwestern end of these outliers to the more continuous bodies is ~7 km; the continuous body has a minimum along-strike length of 26.3 km. If the outliers represent SW-transported segments of the dismembered pluton, a minimum axial extension of 120% is required. Interestingly, the Walker Top Granite in the Big Warrior sheath fold retains relatively undeformed blocky K-feldspar megacrysts, although the matrix is strongly foliated, and contrasts markedly with the strongly mylonitic Walker Top present in Poplar Springs sheath fold. A possible explanation may lie in the lower strength of the enclosing sillimanite schist, the host rock for the Walker Top in the Big Warrior sheath fold, compared with that of the stronger metagraywacke, the host rock for the Walker Top in the Poplar Springs sheath fold.

In the Poplar Springs sheath fold (Fig. 11) of strongly mylonitic Walker Top Granite, we assume a minimum original length for the unsegmented pluton of 25 km, with an additional segmented portion 12.8 km long. This represents a minimal axial elongation of 151%. Segmented Walker Top outliers of the Poplar Springs sheath fold occur immediately northeast of Morganton, some 30 km to the southwest, and we have also observed the likely along-strike continuation of the Poplar Springs sheath fold some 25 km farther northeast south of Wilkesboro (M.P. Gatewood, unpublished data). The minimum axial extension in this shear zone may thus be as much as 178%.

Minimum axial extension in the Ellendale sheath fold (Fig. 11) is more difficult to estimate because the original tabular shape is almost impossible to determine. The horizontal distance from the more linear, SW-trending continuous segment of Toluca Granite to the projected apex involving the dismembered segments to the west, ~9 km, might be used as an indicator of minimum axial extension and transport. Other possible sheath folds, labeled D and E in Fig. 11, defined by dismembered Walker Top and Toluca Granites, are even more difficult to estimate axial extension, so no estimates were made.

While the above estimates of minimum axial sheath fold extension for different IP plutons are only approximations, they demonstrate the highly strained nature of the IP, and likely provide only minimal indications of total strain in these rocks. These estimates made consistent use of all available independent shear-sense data and thus help define the 3-D deformation plan of the IP. From this analysis, however, we can deduce the variation in orientation of the *X*-axis of the strain ellipsoid across the IP. Throughout the IP the *X*-axis is parallel to extension along macro- and mesoscopic sheath fold axes, which are coaxial with L_2 mineral lineations and mesoscopic F_2 fold axes. The *X*-axis thus should conform to the lineation pattern (Fig. 2) across the IP. Actual dimensions of the strain ellipsoid are more difficult to determine. The intact Henderson Gneiss body may provide a macroscopic indication of both the orientation (*X*–NE–SW, *Y*–NW–SE, and *Z*-vertical) and possibly the axial ratio (9:3:1; *X*:*Y*:*Z* from the measured map dimensions of the Henderson Gneiss body, estimated thickness, and bulk $k = 3$–5) of the strain ellipsoid in the western IP. This orientation and ratio are consistent with orientations and ratios of deformed feldspar megacrysts. Estimates of displacements on major IP D_2 faults provide another indication of the magnitude of deformation. Much of the strain in the easternmost IP is probably homogeneous pure shear, but the largest strain component over most of the terrane is inhomogeneous simple shear.

8.2. Fault displacement

Displacements on IP faults must involve both orogen-normal, NW-directed, and orogen-parallel, SW-directed, transport. Many faults in the IP have apparent displacements of only a few kilometers, but actual W- and SW-directed displacements are much larger. Map relationships and displacements parallel to sheath fold axes probably estimate minimum W- and SW-directed displacements on Neoacadian IP faults.

Azcárraga et al. (2002) noted that lateral flow-related displacements in large fault systems are rarely taken into account and may exceed across-strike displacement. 2-D interpretations of the Alto allochthon (Hopson and Hatcher, 1988) (Fig. 1) and other large IP faults like the Six Mile (Griffin, 1974a) and Mill Spring (Davis, 1993a), concluded displacements were all NW-directed and on the order of a few tens of kilometers. Our data indicate SW-directed

transport based on bulk strain in the Henderson Gneiss is 110–240 km along the Neoacadian BFZ. Sheath folds in the BM indicate a minimum of 90 km of SW-directed extension along the Brindle Creek fault. While the Alto allochthon (Fig. 1c) is probably an erosional remnant of the Six Mile thrust sheet, motion of this fault system may have been more SW- than NW-directed. Southwestward emplacement of the Alto allochthon requires at least 50 km of SW-directed transport.

Lateral movement accounts for a significant amount of displacement on Neoacadian IP faults, but NW- and W-directed displacements range from a few kilometers to more than 50 km. Several faults, like the Walhalla nappe and Sugarloaf Mountain fault, decrease displacement and eventually terminate in asymmetric folds. A minimum of 80 km is required to restore the mixed affinity rocks of the Brindle Creek thrust sheet to a position east of the central Piedmont suture between Laurentia and the Carolina terrane. Total displacement on all IP Neoacadian thrusts may thus exceed 400 km, with nearly 200 km associated with dextral strike-slip along the Neoacadian BFZ.

The Toluca and Walker Top Granites occur exclusively in the Brindle Creek thrust sheet suggesting the Cat Square and Tugaloo terranes remained separated until after ~366 Ma (Kalbas, 2003). Peak metamorphic conditions, marked by development of the high temperature mineral lineation, L_2, and migmatite formation throughout the IP, occurred at ~350 Ma. Neoacadian ductile faulting producing a minimum of 400 km displacement via ductile flow at mid-crustal conditions occurred during this 16 m.y. interval.

8.3. Crustal-scale vorticity

Vorticity is an important measure of the noncoaxiality of high-strain zones and, if it can be measured, places at least reasonable limits on the deformation paths in these zones (e.g. Bobyarchick, 1986; Tikoff and Fossen, 1995; Holcombe and Little, 2001; Bailey and Eyster, 2003). Several different techniques, mostly using meso- and microscale structures, have been devised to measure vorticity: deformed markers, porphyroblasts, deformed veins or dikes, crystallographic fabrics, and porphyroclast interactions (Tikoff and Fossen, 1995).

Bobyarchick (1986) suggested that the kinematic vorticity, W_k, depends on the angle α between two eigenvectors and varies as:

$$W_k = \cos\alpha \quad (1)$$

W_k is properly W_m, mean vorticity number, a measure of noncoaxiality (Truesdell, 1954) or W_{ki}, (Tikoff and Fossen, 1995). W_k ranges from zero for pure shear to one for simple shear. Simpson and DePaor (1993) suggested that shear zone boundaries are eigenvectors and thus provide a reference frame to determine vorticity. If so, the angle between the shear zone boundary and other eigenvectors, expressed as deformed markers, can be measured and the kinematic vorticity calculated using Bobyarchick's equation (1). Assumptions required to estimate W_k are plane strain, steady-state deformation, and one direction of ductile flow parallel to and not rotating with respect to the shear zone boundary (Tikoff and Fossen, 1995). Steady-state deformation is probably never achieved in nature, but is a justifiable approximation if deformation is driven by tectonic plate motion that remains constant over time (Tikoff and Fossen, 1995).

While a condition of plane strain may not have existed across the entire IP, we have attempted to determine kinematic vorticities for the flow regimes in the IP using these assumptions. Neoacadian deformation was driven by the accretion of the Carolina terrane microcontinent, with plate interaction that is assumed to have remained constant long enough to develop the penetrative D_2 fabrics in the underlying IP. An additional assumption based on the uniform occurrence of high-grade rocks across the IP core and a lack of pseudotachylite suggests environmental conditions did not change appreciably (or rapidly) during peak deformation that occurred after 366 Ma (age of the Walker Top Granite) and close to the 350–343 Ma time of zircon rim growth (Bream, 2003). Boundary conditions can be defined for the IP: the Carolina terrane forms the southeast and upper boundary, while Neoacadian BFZ forms the lower, northeastern, and northwestern boundary. Finally, ductile flow in the western flank of the IP paralleled the Neoacadian BFZ, which is parallel to the northwestern boundary of the IP, here treated as the shear zone boundary; the angle with other flow orientations can be measured and used to estimate W_k. The dominant mineral lineation L_2 is aligned parallel to the dominant SW-directed transport in the Neoacadian BFZ (Figs. 2d and 12c). This lineation lies in the plane of S_2, and is a C-foliation, so S_2 is considered to be parallel to the shear zone boundary. Resolution of S, C, and C′ is possible in the Henderson Gneiss because it commonly displays a composite fabric (Fig. 3a), but consistent resolution has not been made in other rock units deeper in the IP. For example, in a representative sawed sample of Henderson Gneiss (Fig. 3a), the angle between C and C′ is ~11° (Fig. 3b). If this angle $=\alpha$, $W_k = 0.98$, approaching ideal simple shear behavior (Bobyarchick, 1986). Alternatively, the angle between S and C in this Henderson sample is 24° ($=\theta$). So, using the relationship:

$$\alpha = 90 - 2\theta, \quad (2)$$

(Tikoff and Fossen, 1995), $W_k = 0.74$, suggesting sub-simple shear behavior.

A similar relationship exists across the IP between the dominant foliation and the L_2 mineral stretching lineation, but mesoscopic composite fabrics are not as prominent as in the Henderson Gneiss. Moreover, subsidiary (to the main shear zone boundary) major ductile faults within the IP (Fig. 1) create internal shear zone boundaries that provide an

additional complication for estimating W_k. Our data and observations of structures and fabrics suggest that W_k remains in the sub-simple shear realm across the eastern IP, but approaches ideal simple shear in the Neoacadian BFZ.

9. Appalachian Inner Piedmont and 3-D evolution of orogenic internides

Similar crustal flow patterns tracked by high temperature mineral lineations doubtlessly exist in the deeper parts of most orogens. The curved flow pattern in the Appalachian IP appears unique because of its consistency over at least half of the terrane, and because it is the product of the Neoacadian thermal event. The high temperature mineral lineation in the Appalachian IP tracks a single curved flow regime that reflects: (1) the oblique accretion of the exotic Carolina terrane to distal Laurentian components that comprise the Tugaloo terrane; (2) constriction and SW deflection of otherwise NW- and W-directed flow by the crustal weak zone that became the Neoacadian BFZ; and (3) possible complex curved channel flow (Grudjic et al., 2002) with SW-directed material transport and escape. The curved lineation and flow pattern provides insight into the link between ductile flow and deformation in other ancient orogenic cores and ongoing processes beneath areas of thickened crust in modern orogens.

High temperature, gently to steeply plunging early mineral lineations in both the Lepontine (western Pennine Alps; Merle et al., 1989) and the Suretta nappe (easternmost Pennine Alps; Marquer et al., 1996) record a more uniform, NW-directed linear transport (flow) regime. A similar high temperature, gently plunging, straight lineation pattern exists in the Parry Sound region of the southern Grenville province in Ontario, and has been interpreted by Culshaw et al. (1983) and Hanmer (1988) to record uniform NW transport and ductile flow in central gneiss belt and central metasedimentary belt thrust sheets. The patterns in both the Pennine Alps and southern Grenville province appear relatively simple compared with that in the Appalachian IP, although they are likely the product of heterogeneous simple shear. These segments of both the Alpine and Grenville orogens may have been the product of head-on collision at the time high temperature thrusting occurred. Later events in the Lepontine Alps superposed strike-slip components onto the high temperature elements, particularly along the southern flank, reorienting and transposing them into younger fabrics (Merle et al., 1989).

Robinson and Peterson (2002) have mapped a complex, high temperature mineral lineation pattern from the Pelham dome in central Massachusetts eastward into the Merrimack belt and north into southern New Hampshire. The N–S mineral lineation has been interpreted as the product of crustal flow related to late Pennsylvanian emplacement of the Pelham dome. Another high temperature NW–SE-trending mineral lineation overprinted earlier E–W-trending mineral lineations east of the dome forming a complex swirl pattern, but these lineations formed during the Neoacadian (370–355 Ma) and Acadian (405–385 Ma) high temperature events, respectively. They interpreted these high temperature mineral lineations as the products of long-lived middle and late Paleozoic transpressional (or transtensional) events affecting the core of the New England Appalachians.

Holdsworth and Strachan (1991) reported a curved lineation pattern, NNE- to NNW-trending, in the Caledonides of northeastern Greenland. The pattern is the result of interlinked ductile flow between strike-slip faults and thrusts during Caledonian sinistral transpression. The curved lineation pattern, however, is the result of an early high temperature event and later NNW-directed thrusting unlike the IP lineation pattern, which represents a single high temperature event.

IP mineral lineation pattern and flow paths may be analogous to middle to lower crustal structure beneath the Himalayas. Burn et al. (1985) reported a high temperature, anticlockwise (E–W to N–S) mineral lineation pattern from the Main Central thrust sheet; the result of thrust–wrench coupling along the Main Central thrust in southern Tibet. Recent channel flow models interpret the extrusion of high grade rocks along the Main Central thrust as the result of ductile flow from beneath the Tibetan Plateau, but do not account for the orogen-parallel motion (Beaumont et al., 2001; Grudjic et al., 2002). Curved flow paths, similar to IP flow paths, may exist in the middle to lower crust beneath the eastern and western Himalayan syntaxes associated with lateral escape of continental material along large strike-slip faults. Clark and Royden (2000) predicted clockwise flow of lower crust beneath the eastern Tibetan Plateau, supported by E- to SE-directed velocity vectors from Global Positioning System data (e.g. Burchifiel, 2004). Areas of stronger crust or weaker crust near strike-slip faults may control the flow patterns (Clark and Royden, 2000; Burchifiel, 2004), producing areas of strongly aligned flow similar to the Neoacadian BFZ.

Finally, the relationship of lineation pattern to plate motion is very important. Ellis and Watkinson (1987) proposed a two-stage model for several orogens involving early orogen-parallel, high temperature lineations tracking relative plate motion and late orogen-normal lineations. The curved IP mineral lineation pattern represents one high-grade Neoacadian event. The systematic change in orientation does not represent changes in relative plate motion, but a combination of plate motion, crustal thickening, deflection of material against an oblique buttress, and its lateral escape. Lineation and flow patterns recognized in other orogens are also the result of multiple complex factors.

10. Conclusions

1. Several major Type-F ductile thrusts and several map-scale SW-directed sheath folds that formed at middle to

upper amphibolite facies conditions exist in the northern IP and all formed during the 360–345 Ma Neoacadian event.

2. The Brindle Creek fault, a terrane boundary within the IP juxtaposed Siluro–Devonian metasedimentary rocks and Devonian and younger metaigneous rocks of the eastern IP–Cat Square terrane against Neoproterozoic to Ordovician metasedimentary rocks and Ordovician metaigneous rocks of the western IP–Tugaloo terrane.
3. Sheath-fold geometries vary across the northern IP: those in the western IP are cored by Henderson Gneiss; eastern IP sheath folds are flanked and outlined by thin Devonian granitoid bands. These differences may be related to different amounts of heterogeneous simple shear, original geometries of the plutons being deformed, or both.
4. Noncoaxial ductile flow developed during oblique, W- to NW-directed Neoacadian accretion of the Carolina terrane. Ductile flow rooted in the eastern parts of the northern IP was N- to NW- then W-directed and pushed advancing IP thrust sheets westward. The western part of the northern IP is dominated by a zone of constricted, SW-directed ductile flow, likely the result of buttressing against the Blue Ridge composite terrane adjacent to the Neoacadian BFZ.
5. Estimates of bulk strain suggest the Henderson Gneiss pluton may have a SW-directed axial elongation of 200–486%. The Big Warrior sheath fold, a dismembered Walker Top Granite pluton without large amounts of internal strain, may have undergone 120% of SW-directed axial elongation, while another more internally deformed Walker Top Granite in the Poplar Springs sheath fold may have undergone 178% of SW-directed axial elongation. The curved Ellendale sheath fold that dismembered a Toluca Granite pluton may have 9 km of W- then SW-directed axial elongation. These estimates indicate order-of-magnitude bulk strain for the Neoacadian BFZ in the IP and its SE margin.
6. Net displacement on all Neoacadian faults exceeds 400 km with greater than 200 km of SW-directed displacement along the Neoacadian BFZ. W- to NW-directed displacement ranges from a few kilometers to over 80 km associated with Brindle Creek thrust sheet. Earlier 2-D kinematic models did not recognize the large SW-directed movement component of thrust sheets, and also underestimated displacements.
7. Estimates of kinematic vorticity for the IP place the zone of constricted flow in the realm of simple shear to sub-simple shear. The remainder of the IP probably is in the realm of sub-simple shear.
8. The 3-D Neoacadian deformation plan of the IP (from SE to NW) consisted of curved—N-, to NW-, to W-, to SW-directed—crustal-scale transport and possible channel flow. Similar deformation plans have been recognized in the cores of other well-studied orogens, like the Pennine Alps and southern Grenville province, and should be present in the exposed cores of other orogens.
9. High temperature mineral lineations that track flow patterns in other well-studied orogens appear to have a simpler flow pattern than that in the IP, except for that in southern New England, or are the result of multiple stages of deformation. The curved flow pattern in the Appalachian IP appears unique because of its consistency over such a large terrane, and because it is the product of the Neoacadian thermal event.

Acknowledgements

Funding for this research has been provided by several U.S. National Science Foundation grants (to RDH) and several grants (to RDH) from the EDMAP component of the National Cooperative Geologic Mapping Program, administered by the U.S. Geological Survey. D.C. Curl entered the dip of foliation and plunge of lineation and plotted the histograms in Fig. 2a and c. We appreciate permission from S.E. Bier to use SMC domains IV–VIII in Fig. 7. Reviews by B.R. Bream and L.S. Wiener and journal reviews by R.E. Holdsworth and A.J. Dennis resulted in considerable improvement of the manuscript. We remain culpable for all errors of fact or interpretation.

References

Alsop, G.I., Holdsworth, R.E., 1999. Vergence and facing patterns in large-scale sheath folds. Journal of Structural Geology 21, 1335–1349.

Alsop, G.I., Holdsworth, R.E., 2002. The geometry and kinematics of flow perturbation folds. Tectonophysics 350, 99–125.

Azcárraga, J., Ábalos, B., Ibarguchi, J.I.G., 2002. On the relationship between kilometer-scale sheath folds, ductile thrusts and minor structures in the basal high-pressure units of the Cabo Ortegal complex (NW Spain). Journal of Structural Geology 24, 1971–1989.

Bailey, C.M., Eyster, E.L., 2003. General shear deformation in the Pinaleño Mountains metamorphic core complex, Arizona. Journal of Structural Geology 25, 1883–1892.

Beaumont, C., Jamieson, R.A., Nguyen, M.H., Lee, B., 2001. Himalayan tectonics explained by extrusion of a low-viscosity crustal channel coupled to focused surface denudation. Nature 414, 738–742.

Bentley, R.D., Neathery, T.N., 1970. Geology of the Brevard zone and related rocks of the Inner Piedmont of Alabama. Alabama Geological Society, Eight Annual Field Trip Guidebook.

Bier, S.E., 2001. Geology of the southeastern South Mountains, North Carolina. M.S. thesis, University of Tennessee.

Bier, S.E., Bream, B.R., Hatcher Jr., R.D., 2000. Detailed geologic mapping of the western and central Inner Piedmont, North Carolina. Geological Society of America Abstracts with Programs 32, 234.

Bier, S.E., Bream, B.R., Giorgis, S.D., 2002. Inner Piedmont stratigraphy, metamorphism, and deformation in the Marion–South Mountains area, North Carolina, in: Hatcher Jr., R.D., Bream, B.R. (Eds.), Inner Piedmont geology in the South Mountains–Blue Ridge Foothills and the southwestern Brushy Mountains, central-western North Carolina. Carolina Geological Society Guidebook, pp. 65–100, http://carolinageologicalsociety.org/cgscdguide.htm.

Bobyarchick, A.R., 1986. The eigenvalues of steady flow in Mohr space. Tectonophysics 122, 35–51.

Bream, B.R., 1999. Geology of the Glenwood and Sugar Hill quadrangles, North Carolina, and the structure of the northeast end of the Henderson Gneiss. M.S. thesis, University of Tennessee.

Bream, B.R., 2002. The southern Appalachian Inner Piedmont: new perspectives based on recent detailed geologic mapping, Nd isotopic evidence, and zircon geochronology, in: Hatcher Jr., R.D., Bream, B.R. (Eds.), Inner Piedmont Geology in the South Mountains–Blue Ridge Foothills and the Southwestern Brushy Mountains, Central-Western North Carolina. Carolina Geological Society Guidebook, pp. 45–63, http://carolinageologicalsociety.org/cgscdguide.htm.

Bream, B.R., 2003. Tectonic implications of geochronology and geochemistry of para- and orthogneisses from the southern Appalachian crystalline core. Ph.D. dissertation, University of Tennessee.

Bream, B.R., Hatcher Jr., R.D., 2002. Southern Appalachian terranes amended: timing of accretion and delimiting provenance from new detritral zircon and Nd isotopic data. Geological Society of America Abstracts with Programs 34, 41.

Bream, B.R., Hatcher Jr., R.D., Miller, C.F., Fullagar, P.D., 2000. Paragneiss geochemistry and preliminary ion microprobe geochronology of detrital zircons from the southern Appalachian crystalline core. Geological Society of America Abstracts with Programs 32, 31.

Bream, B.R., Hatcher Jr., R.D., Miller, C.F., Fullagar, P.D., 2001. Geochemistry and provenance of Inner Piedmont paragneisses, NC and SC: evidence for an internal terrane boundary? Geological Society of America Abstracts with Programs 33, 65.

Bream, B.R., Hatcher Jr., R.D., Miller, C.F., Fullagar, P.D., 2004. Detrital zircon ages and ND isotopic data from the southern Appalachian crystalline core, GA–SC–NC–TN: new provenance constraints for Laurentian margin Paragneisses. In: Tollo, R.P., Corriveau, L., McLelland, J., Bartholomew, M.J. (Eds.), Proterozoic Evolution of the Grenville Orogen in North America. Geological Society of America Memoir 197.

Brown, P.M., Burt, E.R., II, Carpenter, P.A., Enos, R.M., Flynt, B.J., Jr, Gallagher, P.E., Horrman, C.W., Merschat, C.E., Wilson, W.F., Parker, J.M., III, 1985. Geologic map of North Carolina. North Carolina Geological Survey, scale 1:500,000.

Bryant, B., Reed, J.C., Jr, 1970. Geology of the Grandfather Mountain window and vicinity, North Carolina and Tennessee. U.S. Geological Survey Professional Paper 615.

Burchifiel, B.C., 2004. New technology; new geological challenges. GSA Today 14, 4–9.

Burn, J.P., Burg, J.P., Ming, C.G., 1985. Strain trajectories above the Main Central thrust (Himalaya) in southern Tibet. Nature 313, 388–390.

Butler, J.R., 1991. Metamorphism, in: Horton Jr., J.W., Zullo, V.A. (Eds.), The Geology of the Carolinas. University of Tennessee Press, pp. 127–141.

Carrigan, C.W., Bream, B.R., Miller, C.F., Hatcher Jr., R.D., 2001. Ion microprobe analyses of zircon rims from the eastern Blue Ridge and Inner Piedmont, NC–SC–GA: implications for the timing of Paleozoic metamorphism in the southern Appalachians. Geological Society of America Abstracts with Programs 33, A42.

Chatterjee, N.D., Johannes, W., 1974. Thermal stability and standard thermodynamic properties of synthetic 2M1 muscovite, $KAl_2AlSi_3O_{10}(OH)_2$. Contributions to Mineralogy and Petrology 48, 119–126.

Clark, M.K., Royden, L.H., 2000. Topographic ooze: building the eastern margin of Tibet by lower crustal flow. Geology 28, 703–709.

Cobbold, P.R., Quinquis, H., 1981. Development of sheath folds in shear regimes. Journal of Structural Geology 2, 119–126.

Conley, J.F., Drummond, K.M., 1981. Geologic map and mineral resources summary of the northeast 1/4 of the Marion quadrangle, North Carolina. North Carolina Geological Survey GM 210-NE, scale 1/24,000.

Culshaw, N.G., Davidson, A., Nadeau, L., 1983. Structural subdivisions of the Grenville province in the Parry Sound–Algonquin region. Geological Survey of Canada Paper 83-1B, 243–252.

Curl, D.C., 1998. Stratigraphy and structure of Wellford and Reidville Quadrangles in part of the eastern Inner Piedmont, near Spartanburg, South Carolina. M.S. thesis, University of Tennessee.

Davis, T.L., 1993a. Lithostratigraphy, structure, and metamorphism of a crystalline thrust terrane, western Inner Piedmont, North Carolina. Ph.D. dissertation, University of Tennessee.

Davis, T.L., 1993b. Geology of the Columbus Promontory, western Piedmont, North Carolina, southern Appalachians, in: Hatcher Jr., R.D., Davis, T.L. (Eds.), Studies of Inner Piedmont Geology with a Focus on the Columbus Promontory. Carolina Geological Society Guidebook. North Carolina Geological Survey, pp. 17–43, http://carolinageologicalsociety.org/cgscdguide.htm.

Davis, T.L., Hatcher Jr., R.D., Liu, A., Tabor, J.R., 1991. Southern Appalachian western Inner Piedmont: a progressive crustal-scale shear zone. Geological Society of America Abstracts with Programs 23, 138.

Dennis, A.J., 1989. Tectogenesis of an accreted terrane: the Carolina arc in the Paleozoic. Ph.D. thesis, University of South Carolina.

Dennis, A.J., Wright, J.C., 1997a. Middle and late Paleozoic monazite U–Pb ages, Inner Piedmont, South Carolina. Geological Society of America Abstracts with Programs 29, 12.

Dennis, A.J., Wright, J.C., 1997b. The Carolina terrane in northwestern South Carolina, U.S.A: Late Precabrian–Cambrian deformation and metamorphism in a peri-Gondwanan oceanic arc. Tectonics 16, 460–473.

Dewey, J.F., Holdsworth, R.E., Strachan, R.A., 1998. Transpression and transtension zones, in: Holdsworth, R.E., Strachan, R.A., Dewey, J.F. (Eds.),Continental Transpressional and Transtensional Tectonics. Geological Society of London Special Publication, 135, pp. 1–14.

Ellis, M., Watkinson, A.J., 1987. Orogen-parallel extension and oblique tectonics: the relationship between stretching lineations and relative plate motions. Geology 15, 1022–1029.

Espenshade, G.H., Rankin, D.W., Shaw, K.W., Neuman, R.B., 1975. Geologic map of the east half of the Winston-Salem quadrangle, North Carolina–Virginia. U.S. Geological Survey Map I-709-B, scale 1:250,000.

Fossen, H., Tikoff, B., 1998. Extended models of transpression and transtension, and application to tectonic settings, in: Holdsworth, R.E., Strachan, R.A., Dewey, J.F. (Eds.), Continental Transpressional and Transtensional Tectonics. Geological Society of London Special Publication, 135, pp. 15–33.

Garihan, J.M., 2001. Observations of the Seneca fault and their implications for thrust sheet emplacement in the Inner Piedmont of the Carolinas. South Carolina Geology 43, 1–13.

Garihan, J.M., Ranson, W.A., Orland, K.A., Preddy, M.S., 1990. Kinematic history of faults in northwestern South Carolina and adjacent North Carolina. South Carolina Geology 33, 18–31.

Garihan, J.M., Preddy, M.S., Ranson, W.A., 1993. Summary of mid-Mesozoic brittle faulting in the Inner Piedmont and nearby Charlotte belt of the Carolinas, in: Hatcher Jr., R.D., Davis, T.L. (Eds.), Studies of Inner Piedmont Geology with a Focus on the Columbus Promontory. Carolina Geological Society Guidebook. North Carolina Geological Survey, pp. 55–65, http://carolinageologicalsociety.org/cgscdguide.htm.

Giorgis, S.D., 1999. Inner Piedmont geology of the northwestern South Mountains near Morganton, North Carolina. M.S. thesis, University of Tennessee.

Giorgis, S.D., Mapes, R.W., Bream, B.R., 2002. The Walker Top Granite: Acadian granitoid or eastern Inner Piedmont basement? In: Hatcher Jr., R.D., Bream, B.R. (Eds.), Inner Piedmont Geology in the South Mountains–Blue Ridge Foothills and the Southwestern Brushy Mountains, Central-Western North Carolina. Carolina Geological Society Guidebook, pp. 33–43, http://carolinageologicalsociety.org/cgscdguide.htm.

Goldsmith, R., 1981. Structural patterns in the Inner Piedmont of the Charlotte and Winston-Salem 2-degree quadrangles, North Carolina and South Carolina, in: Horton Jr., J.W., Butler, J.R., Milton, D.M. (Eds.), Geological

Investigations of the Kings Mountain Belt and Adjacent Areas in the Carolinas. Carolina Geological Society Field Trip Guidebook, pp. 19–27, http://carolinageologicalsociety.org/cgscdguide.htm.

Goldsmith, R., Milton, D.J., Horton, J.W., Jr, 1988. Geologic map of the Charlotte 1-degree×2-degree quadrangle, North Carolina and South Carolina. U.S. Geological Survey Map I-1251-E, scale 1:250,000.

Grant, W.H., 1958. The Geology of Hart County, Georgia. Georgia Geological Survey Bulletin 67.

Griffin Jr., V.S., 1967. Folding styles and migmatization within the Inner Piedmont belt in portions of Anderson, Oconee, and Pickens Counties, South Carolina. South Carolina Division of Geology Geologic Notes 11, 37–52.

Griffin Jr., V.S., 1969. Migmatitic Inner Piedmont belt of northwestern South Carolina. South Carolina Division of Geology Geologic Notes 13, 87–104.

Griffin Jr., V.S., 1971. The Inner Piedmont belt of the southern crystalline Appalachians. Geological Society of America Bulletin 82, 1885–1898.

Griffin Jr., V.S., 1973. Geology of the Old Pickens quadrangle, S.C.: South Carolina Division of Geology MS-18, 54pp., scale 1:24,000.

Griffin Jr., V.S., 1974a. Analysis of the Piedmont in northwest South Carolina. Geological Society of America Bulletin 85, 1123–1138.

Griffin Jr., V.S., 1974. Geology of the Walhalla quadrangle, S.C.: South Carolina Division of Geology MS-19, 53pp., scale 1:24,000.

Grudjic, D., Hollister, L.S., Parrish, R.R., 2002. Himalayan metamorphic sequence as an orogenic channel: insight from Bhutan. Earth and Planetary Science Letters 198, 177–191.

Hadley, J.B., Nelson, A.E., 1971. Geology of the Knoxville 1×2 degree quadrangle, North Carolina, Tennessee, and South Carolina. U.S. Geological Survey Map I-654, scale 1:250,000.

Hanmer, S., 1988. Ductile thrusting at mid-crustal level, southwestern Grenville province. Canadian Journal of Earth Science 25, 1049–1059.

Harper, S.B., Fullagar, P.D., 1981. Rb–Sr ages of granitic gneisses of the Inner Piedmont belt of northwestern North Carolina and southwestern South Carolina. Geological Society of America Bulletin 92, 864–872.

Hatcher Jr., R.D., 1969. Stratigraphy, petrology, and structure of the low rank belt and part of the Blue Ridge of northwestern South Carolina. South Carolina Division of Geology Geologic Notes 13, 105–141.

Hatcher Jr., R.D., 1972. Developmental model for the southern Appalachians. Geological Society of America Bulletin 82, 2735–2760.

Hatcher Jr., R.D., 1974. Introduction to the tectonic history of northeast Georgia. Georgia Geological Society Guidebook 13, 59.

Hatcher Jr., R.D., 1978. Tectonics of the western Piedmont and Blue Ridge: review and speculation. American Journal of Science 278, 276–304.

Hatcher Jr., R.D., 1987. Tectonics of the southern and central Appalachian internides. Annual Review Earth Planetary Science 15, 337–362.

Hatcher Jr., R.D., 1989. Tectonic synthesis of the U.S. Appalachian, in: Hatcher Jr., R.D., Thomas, W.A., Viele, G.W. (Eds.), The Appalachian Ouachita Orogen in the United States, The Geology of North America F-2. Geological Society of America, Boulder, Colorado, pp. 511–535. Chapter 14.

Hatcher Jr., R.D., 1993. Perspective on the tectonics of the Inner Piedmont, southern Appalachians, in: Hatcher Jr., R.D., Davis, T.L. (Eds.), Studies of Inner Piedmont Geology with a Focus on the Columbus Promontory. Carolina Geological Society Guidebook. North Carolina Geological Survey, pp. 17–43, http://carolinageologicalsociety.org/cgscdguide.htm.

Hatcher Jr., R.D., 2001. Rheological partitioning during multiple reactivation of the Palaeozoic Brevard Fault Zone, southern Appalachians, USA, in: Holdsworth, R.E., Strachan, R.A., Macloughlin, J.F., Knipe, R.J. (Eds.),The Nature and Tectonic Significance of Fault Zone Weakening. Geological Society of London Special Publication, 186, pp. 255–269.

Hatcher Jr., R.D., 2002. An Inner Piedmont primer, in: Hatcher Jr., R.D., Bream, B.R. (Eds.), Inner Piedmont Geology in the South Mountains–Blue Ridge Foothills and the Southwestern Brushy Mountains, Central-Western North Carolina. Carolina Geological Society Guidebook, pp. 1–18, http://carolinageologicalsociety.org/cgscdguide.htm.

Hatcher Jr., R.D., Acker, L.L., 1984. Geology of the Salem quadrangle, South Carolina. South Carolina Geological Survey, MS-26, 23pp., scale 1/24,000.

Hatcher Jr., R.D., Goldberg, S.A., 1991. The Blue Ridge geologic province, in: Horton Jr., J.W., Zullo, V.A. (Eds.), The Geology of the Carolinas. University of Tennessee Press, pp. 11–35.

Hatcher Jr., R.D., Hooper, R.J., 1992. Evolution of crystalline thrust sheets in the internal parts of mountain chains, in: McClay, K.R. (Ed.), Thrust Tectonics. Chapman and Hall, London, pp. 217–234.

Hatcher Jr., R.D., Zietz, I., 1980. Tectonic implications of regional aeromagnetic and gravity data from the southern Appalachians, in: Wones, D. (Ed.), Proceedings, The Caledonides in the USA, IGCP Project 27-Caledonide orogen, 1979 Meeting. Blacksburg, Virginia Polytechnic Institute and State University Department of Geological Sciences Memoir, 2, pp. 235–244.

Heyn, T., 1984. Stratigraphic and structural relationships along the southwestern flank of the Sauratown Mountains anticlinorium. M.S. thesis, University of South Carolina.

Hibbard, J., 2000. Docking Carolina: Mid Paleozoic accretion in the southern Appalachians. Geology 28, 127–130.

Hibbard, J.P., Stoddard, E.F., Secor Jr., D.T., Dennis, A.J., 2002. The Carolina zone: overview of Neoproterozoic to early Paleozoic peri-Gondwanan terranes along the eastern flank of the southern Appalachians. Earth Science Reviews 57, 299–339.

Hibbard, J.P., Tracy, R.J., Henika, W.S., 2003. Smith River allochthon: a southern Appalachian peri-Gondwanan terrane emplaced directly on Laurentia? Geology 31, 215–218.

Higgins, M.W., Atkins, R.L., Crawford, T.J., Crawford, R.F., III, Brooks, R., Cook, R.R., 1988. The structure, stratigraphy, tectonostratigraphy, and evolution of the southernmost part of the Appalachian Orogen. U.S. Geological Survey Professional Paper 1475.

Hill, J.C., 1999. Geology of the Marion East quadrangle, North Carolina, and the stratigraphy of the Tallulah Falls Formation in the Chauga belt. M.S. thesis, University of Tennessee.

Holcombe, R.J., Little, T.A., 2001. A sensitive vorticity gauge using rotated porphyroblasts, and its application to rocks adjacent to the Alpine Fault, New Zealand. Journal of Structural Geology 23, 979–989.

Holdaway, M.J., 1971. Stability of andalusite and the aluminum silicate phase diagram. American Journal of Science 271, 97–131.

Holdsworth, R.E., Strachan, R.A., 1991. Interlinked system of ductile strike slip and thrusting formed by Caledonian sinistral transpression in northeastern Greenland. Geology 19, 510–513.

Hopson, J.L., 1984. Stratigraphy and structure of the Alto allochthon, Ayersville quadrangle, Georgia. M.S. thesis, University of South Carolina.

Hopson, J.L., Hatcher Jr., R.D., 1988. Structural and stratigraphic setting of the Alto Allochthon, NE Georgia. Geological Society of America Bulletin 100, 339–350.

Horton Jr., J.W., McConnell, K.I., 1991. The western Piedmont, in: Horton Jr., J.W., Zullo, V.A. (Eds.), The Geology of the Carolinas. University of Tennessee Press, pp. 59–78.

Kalbas, J.L., 2003. Geology of part of the southwestern Brushy Mountains, Inner Piedmont. M.S. thesis, University of Tennessee.

Kalbas, J.L., Bream, B.R., Hatcher Jr., R.D., Maybin, A.H., 2002. Evidence for mafic Ordovician magmatism in the Brushy Mountains, western Inner Piedmont of North Carolina. Geological Society of America Abstracts with Programs 34, 119.

King, P.B., 1955. A geologic section across the southern Appalachians: an outline to the geology in the segment in Tennessee, North Carolina, and South Carolina, in: Russell, R.J. (Ed.), Guides of Southeastern Geology. Geological Society of America, New York, pp. 332–373.

Kohn, M.J., 2001. Timing of arc accretion in the southern Appalachians: perspectives from the Laurentian margin. Geological Society of America Abstracts with Programs 33, 262.

Laubscher, H., 1991. The arc of the western Alps today. Eclogae Geologicae Helvetiae 84, 631–659.

Lemmon, R.E., Dunn, D.E., 1973a. Geologic map and mineral resources of the Bat Cave quadrangle, North Carolina. North Carolina Geological Survey GM 202-NW, scale 1:24,000.

Lemmon, R.E., Dunn, D.E., 1973b. Geologic map and mineral resources of the Fruitland quadrangle, North Carolina. North Carolina Geological Survey GM 202-NW, scale 1:24,000.

Liu, A., 1991. Structural geology and deformation history of the Brevard fault zone, Chauga belt, and Inner Piedmont, northwestern South Carolina and adjacent areas. PhD dissertation, University of Tennessee.

Luth, W.D., Jahns, R.H., Tuttle, O.F., 1964. The granite system at pressures of 4 to 10 kilobars. Journal of Geophysical Research 69, 759–773.

Macedo, J., Marshak, S., 1999. Controls on the geometry of fold-thrust belt salients. Geological Society of America Bulletin 111, 1808–1822.

Mapes, R.W., 2002. Geochemistry and geochronology of mid-Paleozoic granitic plutonism in the southern Appalachian Piedmont terrane, North Carolina–South Carolina–Georgia. M.S. thesis, Vanderbilt University.

Mapes, R.W., Maybin III., A.H., Miller, C.F., Fullagar, P.D., Bream, B.R., 2002. Geochronology and geochemistry of mid Paleozoic granitic magmatism, central and eastern Inner Piedmont, North Carolina and South Carolina. Geological Society of America Abstracts with Programs 34, A-94.

Marquer, D., Challandes, N., Baudin, T., 1996. Shear zone patterns and strain distribution at the scale of a Penninic nappe: the Suretta nappe (eastern Swiss Alps). Journal of Structural Geology 18, 753–764.

Maybin, A.H., III, 1995. Geologic map of the Simpsonville quadrangle, South Carolina. South Carolina Geological Survey Open File Map 92, scale 1:24,000.

Maybin, A.H., III, 1997. Geologic map of the Pelham quadrangle, South Carolina. South Carolina Geological Survey Open File Map, scale 1:24,000.

McConnell, K.I., 1990. Geology and geochronology of the Sauratown Mountains anticlinorium, northwestern North Carolina. Ph.D. dissertation, University of South Carolina.

Merle, O., Cobbold, P.R., Schmid, S., 1989. Tertiary kinematics in the Lepontine dome, in: Coward, M.P., Dietrich, D., Park, R.G. (Eds.), Alpine Tectonics Geological Society of London Special Publication, 45, pp. 113–134.

Merschat, A.J., 2003. Inner Piedmont tectonics in the southwestern Brushy Mountains, North Carolina: field and laboratory data revealing 3-D crustal flow and sillimanite I and II metamorphism. M.S. thesis, University of Tennessee.

Merschat, A.J., Kalbas, J.L., 2002. Geology of the southwestern Brushy Mountains, North Carolina Inner Piedmont: a summary and synthesis of recent studies, in: Hatcher Jr., R.D., Bream, B.R. (Eds.), Inner Piedmont geology in the South Mountains–Blue Ridge Foothills and the southwestern Brushy Mountains, central-western North Carolina. Carolina Geological Society Guidebook, pp. 101–126, http://carolinageologicalsociety.org/cgscdguide.htm.

Mirante, D.C., Patino-Douce, A.E., 2000. Melting and migmatization in the southern Appalachian Inner Piedmont of northeast Georgia; the Athens gneiss. Geological Society of America Abstracts with Programs 33, 297.

Nelson, A.E., Horton, J.W., Clarke, J.W., 1998. Geologic map of the Greenville $1^\circ \times 2^\circ$ quadrangle, Georgia, South Carolina, and North Carolina. U.S. Geological Survey Map I-2175, scale 1:250,000.

Niewendorp, C.A., 1995a. Geology of the Bush River quadrangle, South Carolina. South Carolina Geological Survey Open File Map 84, scale 1:24,000.

Niewendorp, C.A., 1995b. Geology of the Joanna quadrangle, South Carolina. South Carolina Geological Survey Open File Map 85, scale 1:24,000.

Niewendorp, C.A., 1996. Geology of the Laurens North quadrangle, South Carolina. South Carolina Geological Survey Open File Map 89, scale 1:24,000.

Niewendorp, C.A., 1997. Geology of the Paris Mountain quadrangle, South Carolina. South Carolina Geological Survey Open File Map 99, scale 1:24,000.

Niewendorp, C.A., Maybin, A.H., III, 1994a. Geology of the Laurens South quadrangle, South Carolina. South Carolina Geological Survey Open File Map 77, scale 1:24,000.

Niewendorp, C.A., Maybin, A.H., III, 1994b. Geology of the Cross Hill quadrangle, South Carolina. South Carolina Geological Survey Open File Map 78, scale 1:24,000.

Osborne, W.E., Szabo, M.W., Neathery, T.L., Copeland, C.W., Jr, 1988. Geologic map of Alabama, Northeast sheet. Geological Survey of Alabama Special Map 220, scale 1:250,000.

Overstreet, W.C., Yates, R.G., Griffits, W.R., 1963. Geology of the Shelby quadrangle, North Carolina. U.S. Geological Survey Map I-384, scale 1:62,500.

Quinquis, H., Audren, Cl., Brun, J.P., Cobbold, P.R., 1978. Intense progressive shear in Ile de Groix blueschists and compatibility with subduction or obduction. Nature 273, 43–45.

Rankin, D.W., 1975. The continental margin of eastern North America in the southern Appalachians: the opening and closing of the proto-Atlantic Ocean. American Journal of Science 275, 298–336.

Rankin, D.W., Espenshade, G.J., Neuman, R.B., 1972. Geologic map of the west half of the Winston-Salem quadrangle, North Carolina, Virginia, and Tennessee. U.S. Geological Survey Map I-709-A, scale 1:250,000.

Reed, J.C., Bryant, B., 1964. Evidence for strike-slip faulting along the Brevard zone in North Carolina. Geological Society of America Bulletin 75, 1177–1195.

Robinson, P., Peterson, V.L., 2002. Lineation patterns and associated kinematics in central New England: under-reported resource for interpretation of orogenic evolution. Geological Society of America Abstracts with Programs 34, A-29.

Robinson, P., Tucker, R.D., Bradley, D., Berry IV., H.N., Osberg, P.H., 1998. Paleozoic orogens in New England, USA. Geologiska Föreningens Stockholm Forhandlingar 120, 119–148.

Rodgers, J., 1970. The Tectonics of the Appalachians. Wiley-Interscience, New York.

Secor, D.T., Samson, S.L., Snoke, A.W., Palmer, A.R., 1983. Confirmation of the Carolina Slate Belt as an exotic terrane. Science 221, 649–651.

Simpson, C., DePaor, D.G., 1993. Strain and kinematic analysis in general shear zones. Journal of Structural Geology 15, 1–20.

Thompson, A.B., 1982. Dehydration melting of pelitic rocks and generation of H_2O-undersaturated granitic liquids. American Journal of Science 282, 1567–1595.

Tikoff, B., Fossen, H., 1995. The limitations of three-dimensional vorticity analysis. Journal of Structural Geology 17, 1771–1784.

Truesdell, C., 1954. The Kinematics of Vorticity. Indiana University Press, Bloomington, Indiana.

Trümpy, R., 1960. Paleotectonic evolution of the central and western Alps. Geological Society of America Bulletin 71, 843–908.

Trümpy, R., 1980. Geology of Switzerland, a Guide-book. Part A: An Outline of the Geology of Switzerland. Wepf & Co.

Turner, F.J., Weiss, L.E., 1963. Structural Analysis of Metamorphic Tectonites. McGraw-Hill Book Company, New York.

Vauchez, A., Brunel, M., 1988. Polygenic evolution and longitudinal transport within the Henderson mylonitic gneiss, North Carolina (southern Appalachian Piedmont). Geology 16, 101–1014.

Vauchez, A., Babaie, H.A., Babaei, A., 1993. Orogen-parallel tangential motion in the Late Devonian–Early Carboniferous southern Appalachians internides. Canadian Journal of Earth Sciences 30, 1297–1305.

West Jr., T.E., 1996. Geology of the Shoals Junction quadrangle, South Carolina. South Carolina Geological Survey Open File Map 88, scale 1:24,000.

West Jr., T.E., 1997. Structural studies along the Carolina–Inner Piedmont terrane boundary in South Carolina and Georgia: implications for the tectonics of the southern Appalachians. Ph.D. dissertation, University of South Carolina.

Whisonant, J.S., 1979. Geologic map of the SE 1/4 of the Marion quadrangle, North Carolina. North Carolina Geological Survey GM 210-SE, scale 1:24,000.

Williams, H., Hatcher Jr., R.D., 1983. Appalachian suspect terranes, in:

Hatcher Jr., R.D., Williams, H., Zietz, I. (Eds.), Contributions to the Tectonics and Geophysics of Mountain Chains. Geological Society of America Memoir, 158, pp. 33–53.

Williams, S.T., 2000. Structure, stratigraphy, and migmatization in the southwestern South Mountains, North Carolina. M.S. thesis, University of Tennessee.

Willis, J.D., 1984. Geology of the Cross Anchor area—the boundary between the Carolina terrane and Inner Piedmont in northwestern South Carolina. M.S. thesis, University of South Carolina.

Yanagihara, G.M., 1993. Evolution of folds associated with D_2 and D_3 deformation and their relationship with shearing in a part of the Columbus Promontory, North Carolina, in: Hatcher Jr., R.D., Davis, T.L. (Eds.), Studies of Inner Piedmont Geology with a Focus on the Columbus Promontory. Carolina Geological Society Guidebook. North Carolina Geological Survey, pp. 45–54, http://carolinageologicalsociety.org/cgscdguide.htm.

Yanagihara, G.M., 1994. Structure, stratigraphy, and metamorphism of a part of the Columbus Promontory, western Inner Piedmont, North Carolina. M.S. thesis, University of Tennessee.